Goldeneye AB1

Raghav Anand, Alec English, Dante Gao,
Saunon Malekshahi, Rohan Sinha, Noah Stevenson

Faculty Advisor: Professor Stuart Bale, Ph.D.
Director of Space Sciences Laboratory

University of California, Berkeley

NASA Advanced Air Vehicles Design Competition
Supersonic Division

June 12, 2017

Team Members

First-Year Undergraduates

Raghav Anand: Electrical Engineering and Computer Science

Second-Year Undergraduates

Alec English: Physics and Mechanical Engineering

Dante Gao: Mechanical Engineering

Saunon Malekshahi: Mechanical Engineering

Rohan Sinha: Mechanical Engineering and Electrical Engineering and Computer Science

Noah Stevenson: Physics

To whom it may concern,

As the faculty advisor for UC Berkeley's Goldeneye AB1 design team, I affirm the following:

1. All work and writing herein was completed by the students alone, at all stages of the design process, without any professional assistance, and is either original or properly cited, not plagiarized.
2. The students received no NASA funds at any point during the project.
3. I have direct NASA funding of $1,067,947. I am also NASA Principal Investigator on an instrument suite for the Solar Probe Plus mission (Parker Solar Probe), which is funded as a $60 million subcontract from the Applied Physics Laboratory at Johns Hopkins.

Signed,

Stuart D. Bale
Director of Space Sciences Laboratory
Professor of Physics
University of California, Berkeley

Abstract

In October of 2003, the Concorde was retired from service, signaling the end of an era. The airliner was one of only two passenger planes to ever fly supersonic, dominating this market for a quarter-century. Since the Concorde's final flight, commercial aviation has been confined to subsonic aircraft, marking the first time in history that this magnificent industry has regressed technologically. With little incentive, aerospace companies have spent the last decade and a half tweaking and refining the designs of existing aircraft rather than innovating bold new ideas.

However, we are on the cusp of a new chapter in the ongoing history of supersonic flight. In the spirit of inquiry, discovery, and entrepreneurship, we are pleased to present Goldeneye AB1, a supersonic business jet concept that is the first of its kind. A joint venture between the College of Engineering and Space Sciences Laboratory, Goldeneye is the first supersonic commercial plane to feature a variable-geometry wing. With its stowed rotating wing panel, Sears-Haack fuselage, and adjustable engine intake design, the AB1 significantly reduces noise and drastically improves aerodynamic efficiency in comparison to previously conceived supersonic aircraft. While unconventional by design, Goldeneye AB1 presents advancements that are unprecedented in the world of supersonic aviation, rendering it capable of changing the industry forever.

Goldeneye's target cruise speed is Mach 1.7, though it can reliably cruise anywhere from Mach 1.6-1.8. The AB1 attains a total specific fuel consumption of 0.93, with its engines providing 4833.29 lbf (21722 N) of thrust. Goldeneye can traverse its maximum range of 4227 nautical miles in just 3.96 hours, consuming 17853 lb of fuel. Designed to carry up to 12 passengers, the AB1 boasts 2.84 passenger-miles per pound of fuel, making it one of the most efficient supersonic passengers planes ever introduced. Its sleek, versatile, and economical design makes the Goldeneye AB1 the premier contender in the future of supersonic commercial aviation.

1 Introduction

The most successful example of commercial supersonic travel was Concorde, jointly developed by Aérospatiale and the British Aircraft Corporation (BAC). During its 27-year service history, the Concorde became a symbol of innovation and technological prowess. It set countless airspeed and flight duration records, and logged more supersonic flight hours than all other aircraft combined. Despite its impressive track record, the Concorde was eventually forced out of service due to a combination of declining passenger numbers, increasing maintenance and operational costs, and the notorious Air France Flight 4590 incident of 2000. In short, the plane became a financial liability for Air France and British Airways to fly, which ultimately led to its retirement. The "Great White" was more than just an airliner; it was a spectacle to behold. Its sleek ogival delta wing and tailless design set it apart from other aircraft in its class. But above all, the Concorde left its mark by fully embracing the most futuristic visions of commercial travel, inspiring a generation of aviation enthusiasts.

In recent years, aerospace companies have begun to reconsider the allure of supersonic flight. At the forefront of this movement is Boom Technology, a startup whose mission is to design a supersonic civilian jet with the eventual goal of introducing it into the commercial aviation market. Decades of advanced military research, from variable geometry wings to unconventional engine designs, are now being researched again to assist the business development process. Though it is still early, the current technological and economical climate may soon give way to a future where supersonic flight can become a successful industry.

Our vision in developing a supersonic business jet concept is to combine the spirit of innovation demonstrated by the Concorde with careful consideration of the modern need for environmental and economical sustainability, which together lead the way to the reinvigoration of supersonic commercial aviation. Because no competitor has yet succeeded in addressing all of the criteria, Goldeneye AB1 seeks to spearhead the effort and in so doing establish itself as a main contender in this exciting industry.

2 Wing

2.1 Overview

The crowning feature of Goldeneye AB1's design lies in its wing, both figuratively and literally. Throughout the history of supersonic aviation, the greatest challenge has been posed by poor aerodynamic wing efficiency. This is primarily due to the fact that it has proved very difficult to design a wing with a low drag coefficient that simultaneously produces sufficient lift at these speeds. Many different wing configurations have been employed in efforts to achieve this, from the Concorde's classic ogival delta wing to the swept and arrow wings of various supersonic military jets. Notably, the tapered trapezoidal wings of early experimental planes such as the Lockheed F104 and Douglas X-3 yield improved performance at supersonic speeds. While Goldeneye is primarily a supersonic aircraft, it is designed for optimal performance at both subsonic and supersonic speeds, something that has never been done before. To accomplish this requires looking into both the past and present, studying prior wing configurations as well as modern ones. What results is a stunning compromise that pays homage to the past while simultaneously trailblazing a new path for supersonic flight into the future.

Unlike any other variable geometry aircraft, the AB1 is equipped with radially extending panels stowed inside the rear portion of each wing. During subsonic cruise as well as takeoff and landing, these panels are fully extended, forming an ogival delta wing reminiscent of the Concorde's. At supersonic speeds the sector-shaped panels rotate inward about pivots positioned at the back of each wing, adjacent to the fuselage, which transforms the wing into a clipped ogival delta shape (See Figure 1 below). This is discussed extensively in Section 2.4.

2.2 Aerodynamic Theory

An airfoil that performs well at supersonic speeds is a baseline for AB1's success. The NACA 66-206 airfoil is a perfect choice for several reasons. First, it reduces wave drag caused by shock waves that rapidly form as the plane approaches transonic speeds (incidentally, this sudden spike in drag is what creates the sound barrier) [1]. Second, the airfoil has a higher chord to camber ratio than many other supersonic airfoils, which

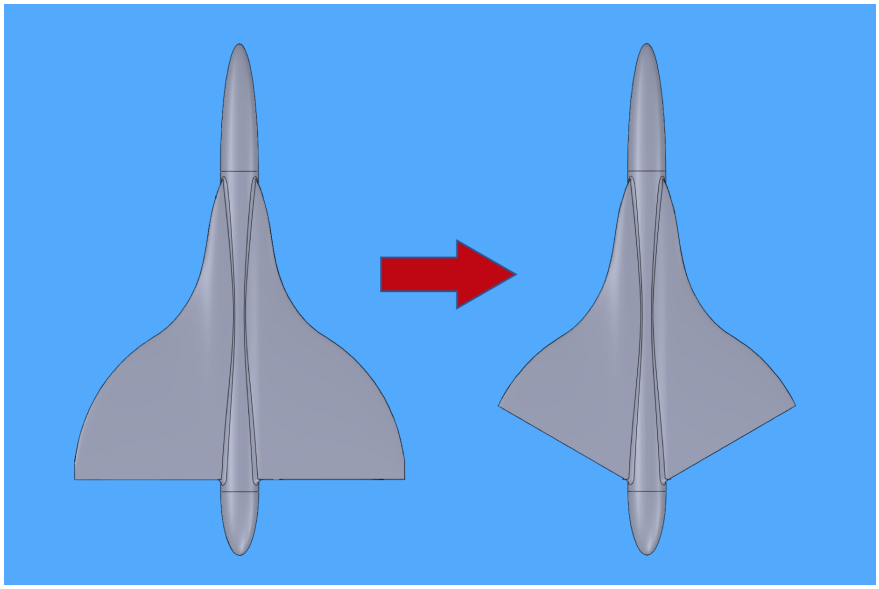

Figure 1: Goldeneye AB1 transforming its wing from an ogival delta to a clipped delta shape.

implies a large surface area for lift at supersonic speeds. Finally, it has a relatively small coefficient of lift at small angles of attack (α), as demonstrated by the plot in Figure 3 of the following page. This reduces the turbulence that the wing experiences during supersonic cruise, ensuring that laminar flow is maintained, which further reduces drag.

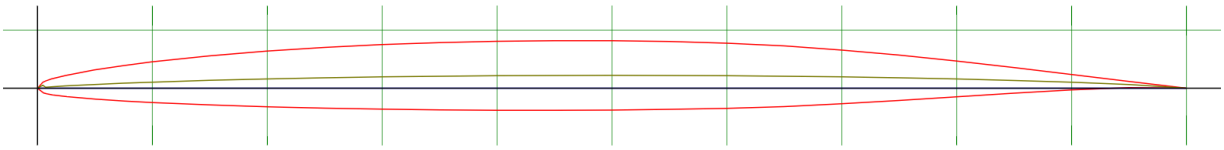

Figure 2: NACA 66-206 Airfoil

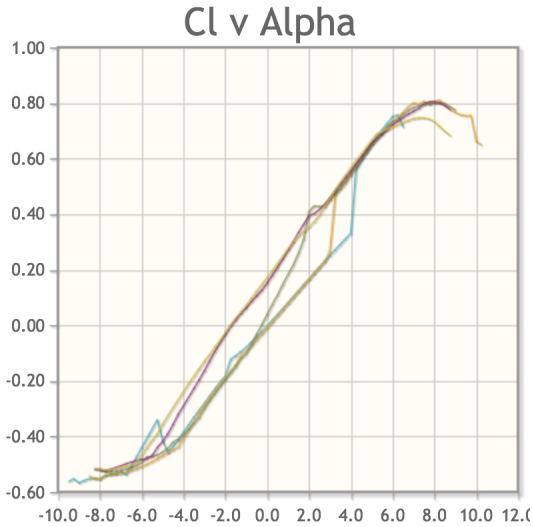

Figure 3: NACA 66-206's lift coefficient (y-axis) vs. attack angle (x-axis) for various Reynolds numbers [15].

During supersonic cruise, the clipped delta wing reduces aerodynamic shear stresses on the surface of the airfoil, enabling the profile of the wing to be thinned. This in turn allows for sharp leading and trailing edges, significantly reducing the wing's drag coefficient. However, during subsonic cruise this wing shape is less aerodynamically efficient and fails to generate sufficient lift. Given the 7,000-meter runway limit, Goldeneye is confined to using existing airport infrastructure and therefore requires the full delta wing in order to provide enough lift to take off and land at subsonic speeds. With its panels fully extended, the wing induces vortex lift [2], a phenomenon that occurs with a swept back wing at high angles of attack. The sharply swept leading edge of the wing induces turbulence that generates vortices across the chord of the wing from the leading edge toward the trailing edge. These vortices are trapped by the outside air, which flows around them and down the back of wing, generating additional lift. The panels supply more wing surface area for the turbulent airflow to act upon, generating additional vortex lift required for flight. Rather ingeniously, the variable geometry of AB1's wing serves to optimize aerodynamic efficiency at both subsonic and supersonic speeds, drastically improving the plane's performance and pioneering a new era of variable geometry in aviation.

2.3 Wing Design Parameters

As previously mentioned, clipped delta wings have been demonstrated to induce less drag than more conventional delta wing geometries at supersonic speeds, making them more efficient in this regard. However, a critical problem for a clipped delta wing at supersonic speeds is its comparatively low lift in the subsonic region. This stems from the fact that the clipped wing has lower planform area than a normal delta wing with the same span and root chord. Many other supersonic wing designs, such as the supersonic laminar trapezoidal wing [3], struggle with the same issue. Since the wing area is decreased, a greater velocity is needed for takeoff, which requires more thrust and consequently increases the amount of noise generated at low altitudes, a major concern for Goldeneye.

Fortunately, the AB1's variable wing geometry allows for the clipped delta wing to be used for supersonic flight, while employing the full ogival delta wing while flying at speeds under the sound barrier, including takeoff and landing. The mechanism by which this is made possible is elaborated upon in Section 2.4.

2.3.1 General Design Parameters

The first parameter that is considered in the wing design is the vertical placement of the wing. Since the chosen airfoil is laminar, the biggest concern in vertical placement is to maintain streamlined airflow along the wing. A Mid-wing placement is more aerodynamically efficient than an upper or lower blend [4]. An added benefit of this configuration is that it keeps the wing closer to the top-mounted engines where it can deflect more of the engine noise away from the ground than a lower mounted wing without being exposed to the high-temperature exhaust gases that an upper wing would experience. The additional support structure required for the mid-wing is best housed in the edges of the elliptical fuselage outside of the cabin, conserving passenger space. Modern materials such as carbon fiber composites can minimize the extra weight of this more involved structure.

Because the drag experienced by the wing increases with wing span dramatically, especially when the wing intersects the Mach cone, a low aspect ratio for the wing is desirable. Furthermore, due to the unique design challenges posed by the variable wing geometry, it is not feasible to implement an angle of twist or dihedral angle that varies along the wing's cross section. Fortunately, this does not pose an issue because these angles are typically small, if not zero, for laminar supersonic wings [5]. In fact, these wings often have zero incidence angle as well to avoid flow separation [6].

2.3.2 Oblique Shock

Though the NACA 66-206 airfoil is highly laminar, oblique shock waves can nevertheless induce large amounts of wave drag on the wing when the critical Mach number is exceeded. The sweep angle of the wing must be designed to avoid these issues as much as possible. The angle of the oblique shock wave is given by [7]:

$$\mu = \sin^{-1} \frac{1}{M}$$

Where M is the Mach number. At Mach 1.7, the average desired cruise speed, this angle is 36 degrees. The sweep angle should be slightly larger than necessary to guarantee minimal shock wave interaction [7]. Therefore, the sweep angle Λ is chosen (with a 10% buffer) to be:

$$\Lambda = 1.1(90^\circ - \mu)$$

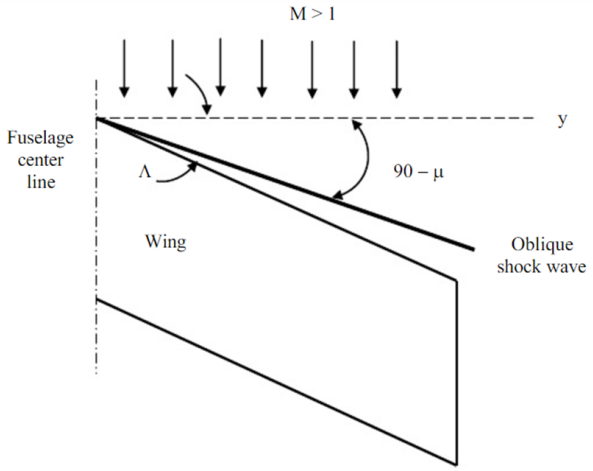

Figure 4: Diagram of a wing with μ, Λ, and oblique shock wave at speeds higher than Mach 1 [7].

This results in a sweep angle of $59.3 \approx 60$ degrees. Similar consideration must be given to the trailing edge, where the wing's disturbance may result in oblique shock waves impacting points farther up on the trailing edge. Because the clipped delta wing is symmetric across its span, the elegance in its design lies in the fact that both the leading and trailing edge approach but do not cross into the zone where oblique shock waves form. Not only do disturbances in flow influence the wing downstream, they may also carry this influence upstream, bounded by the same μ angle [8]. These effects are minimized when the clipped delta wing approaches the oblique shock angle, increasing the stability of the flow. The rear sweep angle can still be decreased to optimize lift when Goldeneye's wing is extended into a full delta geometry. The flow and shock waves along the trailing edge are not negligible because the regions of highest flow velocity around the NACA 66-206 airfoil lie near the trailing edge (See Figure 5 below). However, if the trailing sweep angle is less than 60 degrees, the radial extension cannot be fully stored within the main wing. Therefore, the minimum trailing sweep angle is constrained to 60 degrees, which can be increased to generate more supersonic lift.

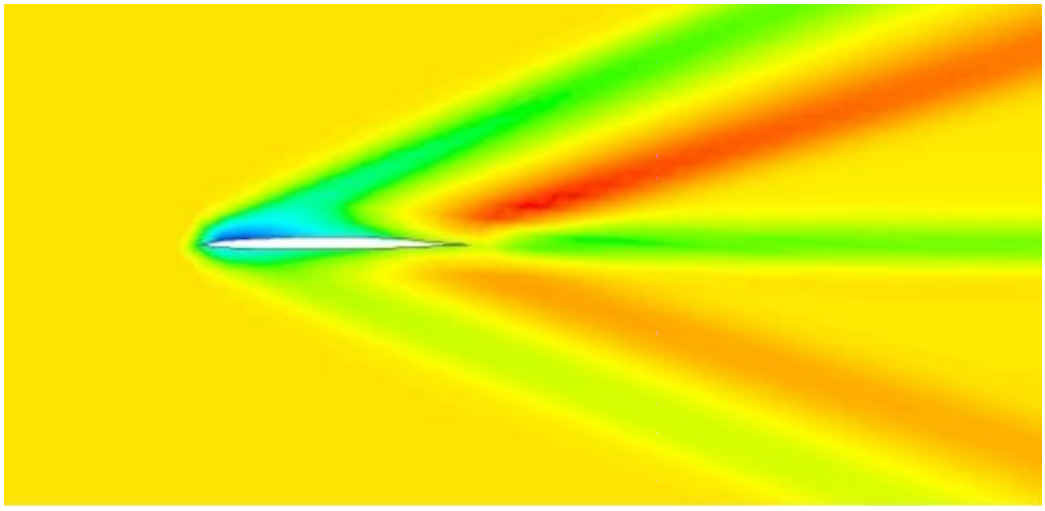

Figure 5: Mach number variation over NACA 66-206 airfoil at Mach 2 [9]. Red represents the highest speeds while blue represents the slowest.

2.3.3 Whitcomb Area Rule

The Whitcomb Area Rule states that in the transonic velocity region, the gradient of the frontal cross sectional area must be minimized to decrease drag and shock wave effects [10]. This logic applies to the supersonic

region to a certain extent as well. To quantify this statement mathematically, if the area is to change at all, then one must find a representative distribution $A(x)$ such that its derivative is minimized at all points along the length of the fuselage, that is:

$$\{A(x) \mid \frac{\mathrm{d}A(x)}{\mathrm{d}x} = \frac{\mathrm{d}A(x)}{\mathrm{d}x}_{\min} \quad \forall\, x \in (a, b)\}$$

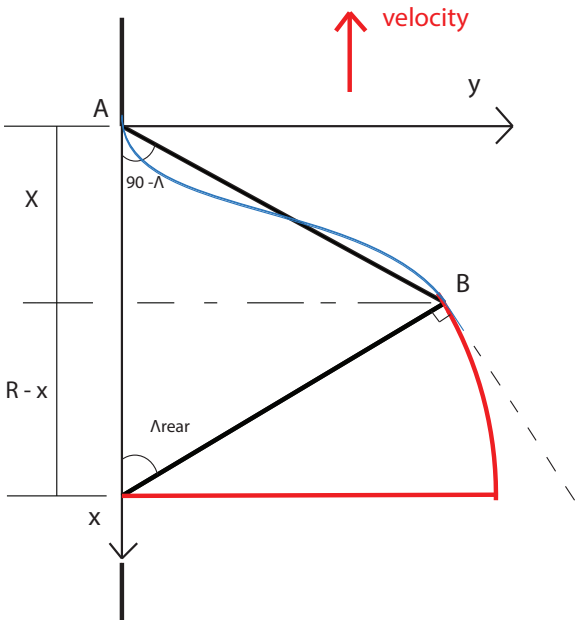

Figure 6: Coordinate System for the Whitcomb Area Rule problem.

Where a and b denote the start and end points of the aircraft fuselage, measured by the x-axis. To account for the area rule, the transition from fuselage to wing must be as smooth as possible. Therefore, a cubic spline $y = ax^3 + bx^2 + cx + d$ is fitted to the leading edge. The spline is constrained to lie between the points $A(0, 0)$ and $B(x_b, y_b)$, the edge of the clipped wing's span. Additionally, the derivative of the spline is constrained to be equal to the slope of the fuselage at A, and to smoothly blend with the radial extension at point B. This makes the derivative at B normal to the slope of the trailing edge, giving

$$x_b = \frac{R\tan(\Lambda_{\text{rear}})}{\tan(\Lambda_{\text{rear}}) - \tan(90 - \Lambda)} \qquad y_b = x_b \tan(90 - \Lambda)$$

Where R is the root chord of the wing. Summarizing these constraints:

$$y(0) = 0 \qquad y(x_b) = y_b \qquad \frac{\mathrm{d}y(0)}{\mathrm{d}x} = 0 \qquad \frac{\mathrm{d}y(x_b)}{\mathrm{d}x}\tan(\Lambda_{rear}) = -1$$

The result is that $c = d = 0$ and:

$$\begin{bmatrix} x_b^3 & x_b^2 \\ 3x_b^2 & 2x_b \end{bmatrix} \begin{bmatrix} a \\ b \end{bmatrix} = \begin{bmatrix} y_b \\ 1/\tan(\Lambda_{rear}) \end{bmatrix}$$

This provides a straightforward way to solve for the leading edge spline function as function of the root chord and rear sweep angle. Now there is a solid framework to prototype the wing; the rear sweep angle can be increased or decreased to optimize the subsonic lift (as it changes the area of the radial wing extension), and the root chord can be increased to boost overall size and lift.

A well-documented benefit of highly swept wings is their induced dihedral effect: "A swept wing produces a negative rolling moment because of a difference in velocity components normal to the leading edge between the left and right wing sections, hence, a swept wing may not need a dihedral or anhedral to satisfy lateral-directional stability requirements" [11].

2.3.4 Center of Pressure Optimization

There are a number of other perks generated by the ability to switch from a clipped delta to a full delta wing shape. One of these presents itself when tackling one of the major design concerns faced by the Concorde: its shifting center of pressure. As aircraft velocity increases, the x-coordinate of the wing's center of pressure shifts toward the trailing edge (see Figure 6 above). As such, the center of pressure of the Concorde would shift around 6 feet between takeoff and supersonic cruise [12]. To account for this, an elaborate fuel pumping control system was designed to distribute fuel mass to move the center of gravity of the aircraft and maintain stability. This greatly complicated the design, increasing cost as well as wasting the energy required to pump 20 tons of fuel around the plane.

This issue is circumvented by the variable wing geometry as the radial extension increases pressure near the trailing edge of the wing at low speeds, moving the center of pressure backward. Since the extension retracts during supersonic flight, the loss of this added pressure offsets the natural rearward displacement of the pressure center at supersonic speeds. The result is a design that can be optimized to keep the center of pressure in approximately the same location at both subsonic and supersonic velocities. Mathematically, the wing would be designed such that:

$$\frac{\iint_{S_1} x \cdot P_{\text{supercruise}}(x,y)\mathrm{d}x\mathrm{d}y}{\iint_{S_1} P_{\text{supercruise}}(x,y)\mathrm{d}x\mathrm{d}y} = \frac{\iint_{S_2} x \cdot P_{\text{subsonic}}(x,y)\mathrm{d}x\mathrm{d}y}{\iint_{S_2} P_{\text{subsonic}}(x,y)\mathrm{d}x\mathrm{d}y}$$

where $P_{\text{supercruise}}$ and P_{subsonic} are the pressure distributions along the wing at supersonic cruise and a representative subsonic velocity, S_1 is the clipped delta wing planform area, and S_2 is the full delta wing planform area [13]. This optimization cannot be performed, because realistic pressure distributions are not ascertainable by experiment and simulation tools equipped for such complexity are not accessible to the team.

2.3.5 Thickness Ratio Optimization

Another benefit of the variable wing geometry is the opportunity to change the thickness ratio of the airfoil. Since the extension is stored within the wing, as soon as it is deployed, the hinges on the trailing edge of the clipped wing open to allow the extension to protrude farther (see Section 2.4). Therefore, the 6% thickness ratio of the NACA airfoil can be changed during subsonic flight. The ideal thickness ratio for that condition is governed by the Torenbeek equation [14]:

$$\frac{t}{c} = 0.30\left[\left(1 - \left(\frac{5+M^2}{5+(M^*)^2}\right)^{3.5}\right)\frac{\sqrt{1-M^2}}{M^2}\right]^{2/3}$$

Where $\frac{t}{c}$ is the thickness ration, M is the mach number, and M^* is some constant unique to each airfoil. This allows the extension-modified airfoil to have a thickness ratio optimized for any subsonic Mach number.

2.3.6 Wing Comparisons

One final comparison is noteworthy to be drawn between the proposed clipped delta wing, the Concorde's full delta wing, and the laminar trapezoidal wing of the Aerion and Boom supersonic aircraft. The full delta geometry of Goldeneye's wing is extremely similar to the ogival delta wing of the Concorde. However, the Concorde's wing is often categorized as a variable sweep wing, which struggled to balance supersonic and subsonic efficiency. The Aerion's laminar trapezoidal supersonic wing provides less lift at subsonic speeds, which bears responsibility for undesirable noise, runway, thrust and weight characteristics. However, the Aerion demonstrates that, given a highly laminar airfoil, oblique shock waves are perhaps not quite as significant a

concern. This means that the front sweep angle can be tweaked as well in finalizing a scaled version of the wing to suit the lift requirements of the aircraft (See Section 5.1). Thus, Goldeneye's variable geometry wing cleverly manages to capture the best of all worlds.

2.4 Mechanism

Historically, aircraft variable wing geometry has proved costly and technologically complex. Previous mechanism designs often malfunctioned, broke, or had such fundamental flaws that their production was discontinued. Most variable geometry designs consist of a single pin joint several feet outboard of the fuselage about which the entire wing rotates. This implementation is structurally vulnerable because it subjects the pin to immense shear stress from the moment created by the weight of the fuselage and the wing's lift force.

Goldeneye's design seeks to eliminate this common design flaw. Similar to a Fowler flap [16], the panel is secured with rollers that are fixed to its bottom side and slotted into two radial tracks grooved into the bottom of the interior of the wing. To move the panel, a straight groove in the top of the wing interior houses a linear hydraulic actuator that is attached by pivots to the foremost straight edge of the panel on one end and to the edge of the wing, adjacent to the fuselage, on the other end. As the aircraft transitions between subsonic and supersonic cruise, the actuators retract or extend within their grooves, rolling the panel along the curved tracks radially until the desired wing shape is reached (see Figure 7 below).

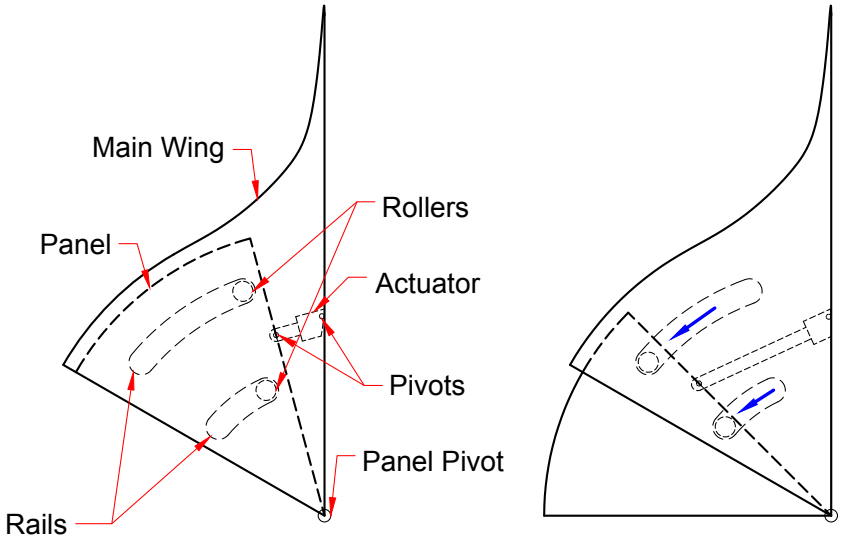

Figure 7: Top view of the left wing, revealing the interior design of the radial panel mechanism as it extends outward. Wing shape and mechanism size not to scale.

To allow for this motion, the trailing edge of the clipped wing has thin flaps that are hinged to the back of the wing at the highest and lowest points of the clipped face for ease of motion. These hinged flaps allow the end of the interior channel to narrow or widen to accommodate the increasing or decreasing thickness of the exposed region of the panel. This maintains a smooth curve so as not to disrupt airflow over the wing.
To preserve the airfoil's shape, the panel is designed such that it serves as the back of the airfoil when fully extended, complementing the front of the airfoil from the fore region of the wing. This requires that the panel's airfoil axis be parallel to the fuselage's when it is fully extended. Consequently, when the panel is fully retracted, its airfoil axis is offset from the fuselage's by the angle between the trailing edge of the clipped wing and a line perpendicular to the fuselage. This issue is resolved by installing the panel such that it is always at least slightly extended from the wing interior, even when retracted (See Figure 8 on the following page). It should be noted that the trailing edges of the main wing and panel remain adjacent when the panel

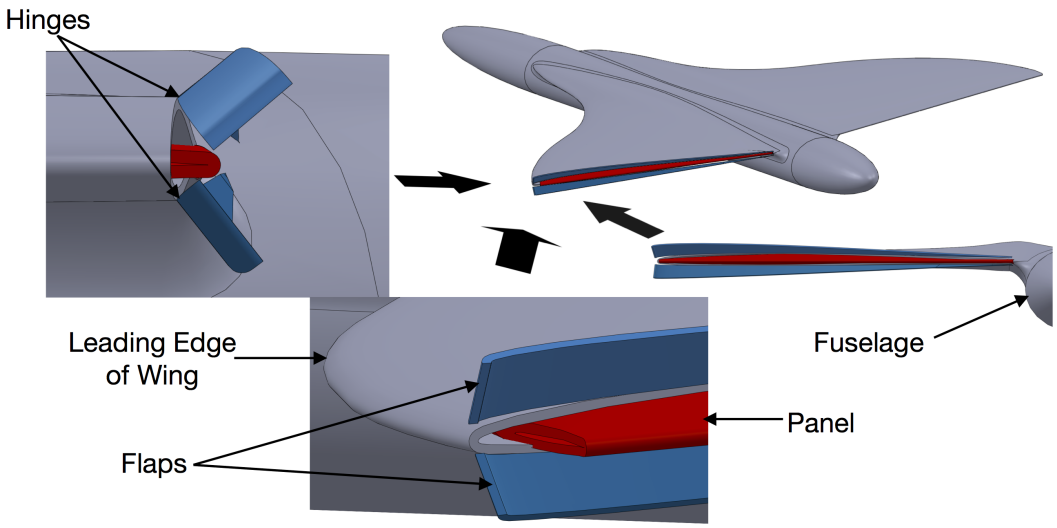

(a) Panel retracted, with hinges opened to allow for extension.

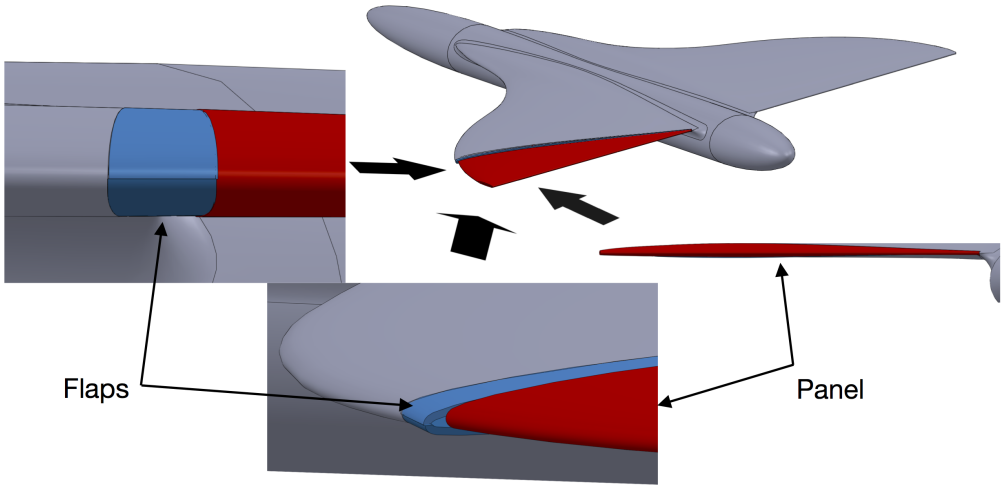

(b) Panel extended, with hinges closed to maintain smooth wing surface.

Figure 8: Side, oblique, and back views of the panel, depicted as it extends outward. Note that the panel starts slightly extended from the wing's channel even when fully retracted.

is fully retracted, and that the hinged flaps lie just on top and bottom of the panel's trailing edge in this configuration. In this way, Goldeneye's wings have a smooth, continuous airfoil at all times.

2.5 Control Surfaces

One of the main concerns arising from the use of variable geometry wings is how to implement the control surfaces that roll and pitch the aircraft. Conventionally, ailerons are mounted on the trailing edge of the wing to

control the rolling moment. However, this configuration is only effective for Goldeneye during subsonic flight. This is because the radial panel is extended at low speeds and ailerons may only be placed on the trailing edge of the panel since the main wing features hinged flaps that preserve the airfoil's shape. While roll control is most important during subsonic flight when AB1 is doing the majority of its maneuvering, it will spend much time at supersonic cruise, making it necessary to better control AB1's roll. To address this problem, inspiration can be gleaned from the Grumman F-14, a supersonic fighter jet with variable-sweep wings. This aircraft uses wing-mounted spoilers instead of ailerons to enable roll control, even during supersonic flight. However, the spoilers must be disabled if the plane's sweep angle exceeds 57° [17]. Fortunately, Goldeneye's variable geometry does not affect its sweep angle, allowing the installation of wing spoilers that are functional during both subsonic and supersonic flight.

The Concorde had the luxury of ailerons as a primary control surface, operating them differentially to generate a rolling moment and symmetrically for a pitching moment. Furthermore, it did not require a horizontal stabilizer due to the added stability of the delta wing at supersonic speeds. On the contrary, Goldeneye is much less horizontally sound during supersonic cruise because of its clipped delta wing, trading stability for reduced drag. Therefore, a separate mechanism is required for both horizontal stability and to control pitch, which the spoilers do not address. A canard seems to be the simplest and most effective way to achieve this, discussed further in a later section.

2.6 Materials & Structure

The wing's frame consists of tapered steel cross sections joined by two titanium spars. Its surface is coated with aluminum alloy 7075-O, a common industry-grade aviation material. The steel tracks for the extension mechanism are attached to the wing's cross-sections via titanium fasteners, atop which the radial panel rests. The panel is comprised of carbon composite cross sections united by a spar to reduce weight and is stored in the empty space between the wing's cross sections.

3 Fuselage

3.1 Cabin

The length and cross-sectional area of Goldeneye AB1's cabin is dictated by the passenger load for which the plane is designed. Holding up to 12 passengers, Goldeneye's cabin is an elliptical prism measuring 3 meters along its major axis, 2.4 meters along its minor axis, and 10 meters in length, with a shell thickness of 2 centimeters. The floor is positioned 2 meters (6.56 feet) below the apex of the cabin for optimal headroom. The elliptical cross section serves to maximize passenger space inside the cabin, providing more width and storage for baggage and other cargo. In addition to increasing the cabin's volume, this shape also provides for a more seamless integration with a mid-wing mount that is not only more aesthetically pleasing but also reduces interference drag due to the interaction of airflow streamlines between the wing and fuselage [19].

Underneath the cabin, AB1's underbelly serves primarily as fuel storage. Because it is a business jet, Goldeneye is not concerned with providing excess cargo space, though the very front of the underbelly features a sizable volume for this purpose. Aft of this space, three equally sized fuel tanks line the rest of the underbelly, adjacent from front to back. The tanks are connected by valves to control the drainage rate. Normally, the tanks empty evenly in order to keep the plane's center of gravity stable, but this can be adjusted accordingly if need be.

3.2 Nose and Tail

Goldeneye's fuselage is designed around the aerodynamic principles governing supersonic flow in order to minimize drag at supersonic speeds. The nose and tail are both formed from half of a Sears-Haack body, mounted directly fore and aft of the cabin, respectively.

The Sears-Haack body is a geometric shape that theoretically minimizes wave drag in supersonic flow for a given length [20], making it a perfect choice for Goldeneye's nose and tail. These features differ from the ideal

Sears-Haack half body in that their cross sections are elliptical instead of circular. Fortunately, this does not alter their construction process too drastically. The equation for the radius of a circular Sears-Haack cross section is given by:

$$r(x) = R_{\max}\left[\frac{2x}{L}\left(1 - \frac{x}{2L}\right)\right]^{3/4}$$

where x is the distance from the tip of the half-body, L is the length of the half-body, and $R_{\max}$ is the maximum radius of the half-body, taken to be the semi-major axis of the fuselage (1.5 meters) to ensure that the components mesh together smoothly. First, the nose and tail lengths are chosen. Then, to preserve the cross sections as ellipses, $r(x)$ is used to calculate the semi-major axes of the cross sections at set intervals. The full ellipses are constructed by fixing their eccentricity at the same value as the cabin ellipse, which is found by $e = \sqrt{1 - \frac{b^2}{a^2}} = 0.6$, where a is the semi-major axis (1.5 meters) and b is the semi-minor axis (1.2 meters). Finally, the cross sections can be connected into one smooth shape by a loft (Figure 9 below).

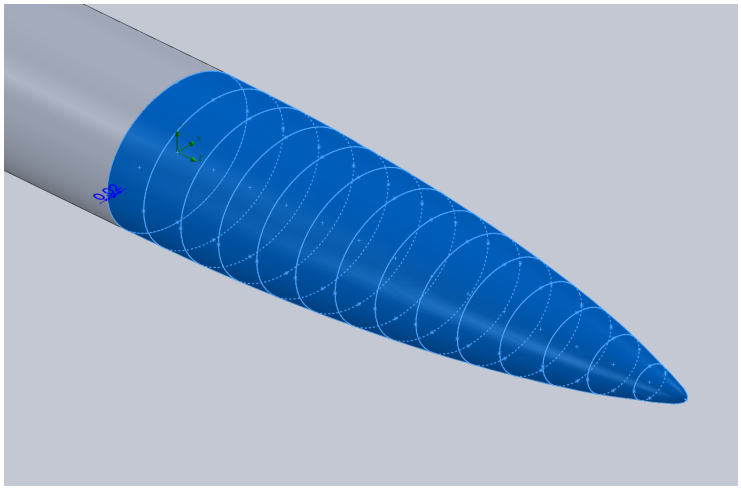

Figure 9: Fusing a 10m nose to the fuselage by lofting ellipses at regular intervals.

Now all that is needed are lengths for the nose and tail, whose optimal values can be determined from flow simulations in SolidWorks. As expected, the longer the Sears-Haack body, the more gradually it tapers to a point and the less drag present. However, this also incurs more weight and therefore more lift required, so a decision must be made to compromise between the two. Because the plane will spend the majority of its flight time traveling at supersonic speeds, drag should be minimized for a Mach number of 1.7, the mean target speed for the aircraft. Assuming that Goldeneye travels at an altitude of 18,000 meters, roughly the maximum height at which the Concorde flew, the average air pressure and temperature would be about 7500 Pa and 215 K, respectively. Inputting this information into the simulation parameters and arbitrarily fixing the tail length to 5 meters, we can compare the average drag force on the entire fuselage to the volume of the material making up the nose, since volume has a one-to-one correspondence with mass, regardless of material. This allows for the fuselage material to be determined later. The more voluminous the nose, the more lift will be required for the plane to fly. Plotting the results averaged after 5 trials for each nose length at 1-meter intervals from 7 to 12 meters, the relationship between these properties appears to be best modeled by a cubic function in this range, displayed on the chart below (Figure 10a).

The nose length corresponding to the inflection point of the cubic function is the best choice for the fuselage because beyond this nose length the mass begins to increase more significantly rapidly as drag decreases. This point can be found by finding the root of the function's second derivative, which corresponds to a value of 25.41 kN. Finally, using our drag values to interpolate between the 9m and 10m nose lengths the optimal nose length is found to be 9.2 meters.

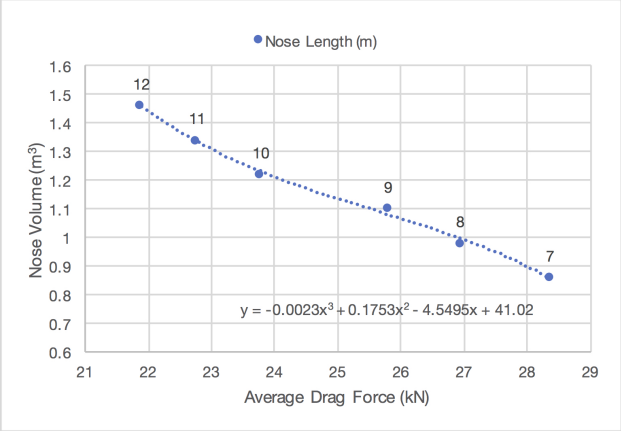

(a) Nose volume vs. average fuselage drag force for various nose lengths with a fixed 5-meter tail.

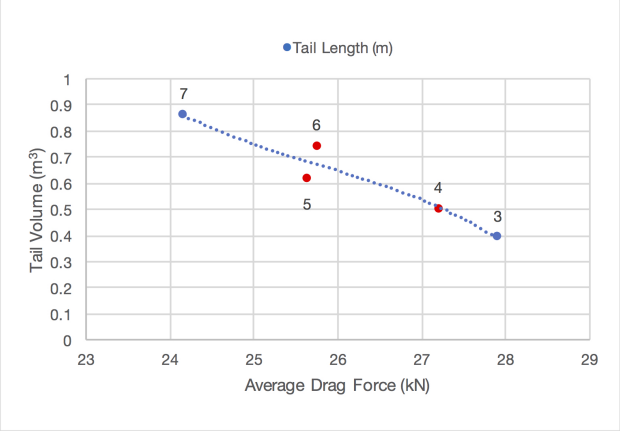

(b) Tail volume vs. average fuselage drag force for various tail lengths with a 9.2-meter nose. Red data points illustrate that the properties are not related by a function.

Now that we have a fixed nose length, the same analysis can be performed to find a corresponding optimal tail length. Running the flow simulations with the same environmental properties and a 9.2-meter nose, the average drag force can be calculated at 1-meter intervals for tail lengths from 3 to 7 meters. Interestingly, when the drag values are plotted against the tail volume, the relationship between these values is not the same as with the nose. This is likely due to the nose interfering with the flow before it reaches the tail and therefore perturbing the results. Unfortunately, the data do not appear to be modeled by any function, since the drag force decreases from the 4-meter to the 5-meter nose, but then increases when the nose is extended to 6 meters (Figure 10b above). One can quickly see that no matter how the points are connected, the plot fails the vertical line test (the data points of interest are highlighted in red). Without a clear understanding of the relationship between the drag and the tail volume, the most logical choice for the tail length is in the vicinity of the 5-meter point, where the drag is lower than expected based on the rest of the plot. Setting the tail length to 4.8 meters, the overall length of AB1 is a nice round 24 meters.

3.3 Cockpit

The cockpit is simply an extension of the cabin, ending where the cabin floor meets the nose when extended forward. The bottom dimension is thus preserved, meaning that the perpendicular distance from the cockpit floor to the cabin apex is still 2 meters. However, the cockpit roof must conform to the top of the nose, tapering down until it reaches the same forward distance as the floor. The resulting loss of head space does not pose an issue since the pilot and co-pilot are seated at all times inside the cockpit. Unlike the Concorde, AB1's windshield is seamlessly integrated with the nose to preserve the Sears-Haack shape and minimize drag at a minimum. At high angles of attack during takeoff and landing, this design poses a visibility issue. To avoid a complicated and expensive design like the Concorde's droop nose, Goldeneye is equipped with cameras to aid the pilot, a simple solution to an important problem.

3.4 Materials

The skin of an aircraft, especially on the fuselage, experiences extreme shear stresses and temperature fluctuations during flight. Thus, materials making up the external structure of an aircraft are characterized by creep resistance, high tensile strength, and a low thermal expansion coefficient. Furthermore, they must not be very dense to reduce the weight of the frame. Traditionally, aluminum alloys have been used in these applications as they possess many of the aforementioned characteristics.

However, supersonic flight poses additional challenges. To reach such high speeds, supersonic aircraft must fly at higher altitudes than their subsonic counterparts in order to take advantage of the thinner atmosphere.

This creates larger hoop and radial stresses within the fuselage, as well as much higher thermal stresses due to the adiabatic compression of the incoming air.

For these high performance requirements titanium alloys make good candidates, namely, Ti-6Al-4V. This alloy has a very desirable strength-to-weight ratio, a low thermal expansion coefficient, and significant fatigue resistance. Additionally, it is highly resistant to corrosion. In order to enhance the strength of the alloy, it may be nitrided to produce a case-hardened surface, which preserves the alloy's ductility under bending moments while improving its fatigue resistance by introducing compressive stresses at the surface that limit the rate of crack growth.

Ti-6Al-4V is chosen to construct Goldeneye's fuselage over other alloys, including Hiduminium, Al-Sc alloys, and 7068 aluminum, due to its superior tensile strength and lower cost. The alloy is most critically needed near high-stress areas of the airframe, such as the wing root, nose tip, and engine casing. In areas where stresses are generally lower, it may be permissible to employ other alloys to reduce weight at a slight cost of strength. For example, Hiduminium, along with other aluminum alloys such as 6061, is perfectly suitable for structural components within the fuselage. Struts, supports, and other features within the aircraft are not impacted by environmental factors, and therefore the selection criteria for these parts is less rigorous.

Composite materials, especially laminates and sandwich panels, may serve a purpose in the fuselage as well. Sandwich-structured composites and fiber-reinforced polymers have the ability to produce very strong materials, but also come with several drawbacks. The construction of sandwich panels and fibrous composites in a matrix implies that the material is much weaker in one direction. For example, care must be taken to ensure that the facesheets of a sandwich panel do not detach from the core. The mechanical properties of fiber-reinforced epoxies vary greatly depending on whether the applied stress is parallel or perpendicular to the direction of the fibers. Therefore, unless the full extent of the loading condition is considered beforehand through much deeper analysis, it is impractical to rely heavily on such materials.

4 Propulsion

Goldeneye's propulsion system is modeled after an existing engine, which is first scaled to fit on the plane and then tweaked to improve performance. The engine of choice is the Olympus 610 of the Concorde B, an improved but unfinished revision of the original Concorde's design. This engine is one of only two ever successfully built to propel a supersonic commercial plane[1]. Olympus 610 is the result of years of research and development to optimize long-range engine performance, which addresses the low-range barrier that most other supersonic propulsion systems face, making it a good starting point to scale into an analog engine for Goldeneye.

4.1 Engine Dimensions & Supersonic Thrust Calculations

A number of scaling arguments were used to tailor the Olympus engine to Goldeneye's fuselage and wings. Given the much smaller size of the plane relative to the Concorde, a two-engine setup makes the most sense as opposed to the Concorde's four-engine layout.

The following arguments are included to mathematically justify the engine scaling process [21]:

$s \equiv$ Scale Factor $\qquad L \equiv$ Engine Length
$D \equiv$ Engine Diameter $\qquad W \equiv$ Engine Weight
$T \equiv$ Thrust

$$s = \frac{T_{\text{reqd}}}{T_{\text{data}}} \qquad L_{\text{reqd}} = L_{\text{data}} \cdot s^{0.4} \qquad D_{\text{reqd}} = D_{\text{data}} \cdot s^{0.5} \qquad W_{\text{reqd}} = W_{\text{data}} \cdot s^{1.1}$$

where the subscript *reqd* represents values for Goldeneye's engine and *data* represents values for the Olympus engine.

[1] The other being the Kuznetsov NK-144 of the Russian-manufactured Tupolev Tu-144

To calculate the dimensions of the scaled engine, an estimate of the thrust during level flight is required, which can be found by [23]:

$$T_{\text{reqd}} = \frac{W}{C_L/C_D}$$

where C_L is the lift coefficient and C_D is the drag coefficient.

To account for deviations from the ideal conditions that the previous equations assume (a constant drag force that does not account for the plane's acceleration), the theoretical required thrust is calculated for the Concorde. Observing that this formula underestimates the required thrust by 11.98%, a correction can be made to more accurately calculate Goldeneye's required thrust:

$$T_{\text{reqd}} = 1.1198 \cdot \frac{W}{C_L/C_D}$$

Because Goldeneye's weight is a bit vague due to different materials considerations, it is a good idea to use a similarly sized subsonic plane, the Gulfstream G280 [24], to provide an upper bound for Goldeneye's weight (18000 kg). The coefficient of lift (0.125) and drag (0.0175) are taken from the Concorde's supersonic cruise as a worst-case estimate, since the fuselage and wings of Goldeneye are more optimized for streamlined flight than the Concorde's. Plugging these numbers in, it is calculated that $T_{\text{reqd}} = 21722\,\text{N}$ and therefore both engines must supply half this thrust, 10861 N. Finally, with this value the scaling factor and dimensions of the engine are found:

$$s = 0.2395 \qquad L_{\text{reqd}} = 3.34\,\text{m} \qquad D_{\text{reqd}} = 0.684\,\text{m} \qquad W_{\text{reqd}} = 660\,\text{kg}$$

4.2 Afterburner Performance

Planes with the ability to supercruise, that is, to fly at supersonic speeds without an afterburner, can either use an afterburner to break the sound barrier or not. This is an substantial decision to make because the use of an afterburner drastically increases fuel consumption.However, the advantage of an afterburner is that it shortens the duration of time required to break the sound barrier. As Figure 10 indicates, most supersonic airfoils experience a sharp increase in drag as the plane approaches the speed of sound, followed by a rapid decline in drag [26]. Consequently, many supersonic planes use an afterburner because the time saved as the plane transitions from subsonic to supersonic velocity (Figure 11) makes up for the short, intense burst of fuel consumption and actually conserves fuel overall. This phenomenon is illustrated by the plots below and suggests that Goldeneye should employ an afterburner to break the sound barrier more efficiently.

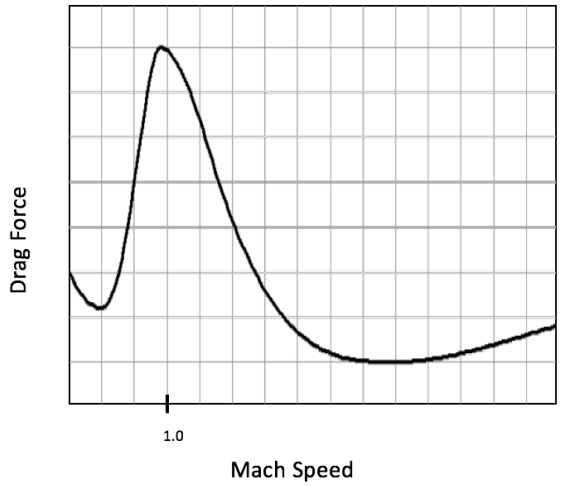

Figure 10: Drag vs. Mach number for a typical supersonic jet [26].

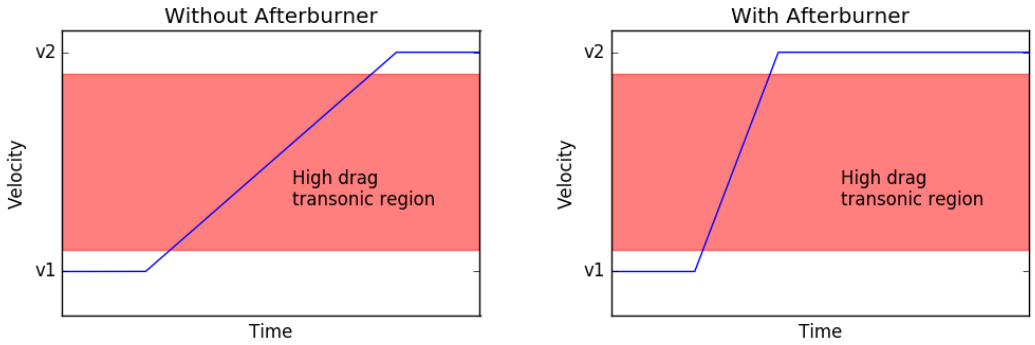

Figure 11: Plane velocity vs. time elapsed while breaking the sound barrier without and with an afterburner.

4.3 Inlet

Recent supersonic designs feature intake ramps because of their adaptability over vast ranges of conditions, angles of attack, and mass flows. The variable ramp offers short-term high efficiency propulsion over a wide extent of supersonic speeds. This is an important characteristic for fighter aircraft because they often accelerate to supersonic speeds for minutes at a time and perform sharp maneuvers. Under these circumstances, air mass spill is severe, often causing shadows and gaps to form in the airflow due to directional changes. Fighter jets must also execute supersonic bursts under whatever conditions that the situation at hand requires. This need for adaptability makes the high weight and complexity of ramp inlets worthwhile.

However, a supersonic business jet's main function is to sustain supersonic cruise for long periods of time, not short intervals. For this reason, Goldeneye's inlet design consists of a moderate spike intake, despite this being a largely untested concept. A spike intake, featuring a conical section extending forward from the inlet of the engine, is advantageous for many reasons. It does not disturb airflow to the engine, is lightweight and compact, and reduces construction and maintenance costs. Furthermore, while it may be extensive, because the ducting's sole purpose is to separate the interior and exterior flow, the engine can be quite lengthy without significant increases in drag or weight.

The mechanism resembles those of the MiG-21 or SR-71 engines, so the forward end of the engine can be

modelled as a cylinder with a conical spike. Past aircraft with engines situated inside the fuselage such as the Mach-2-capable English Electric Lightning have used the cone to store radar equipment, but it is hollow on Goldeneye for weight reduction. In addition, the radar's performance is heightened when it is placed father forward in the aircraft. A simple translational mechanism moves the cone back and forth to adjust the intake cross section. To provide a shallow angle of attack, the cone length is 3 meters and cone radius is 0.335 meters, which is almost completely inside of the 4-meter long ducting area when retracted. At subsonic speeds, the retracted cone compresses the mass that flows into the frontal section, which then passes into the engine cycle. This allows for high total pressure recovery and inlet efficiency, as defined below [49]:

$P_{\mathrm{i}} \equiv$ Intake Pressure	$P_{\mathrm{f}} \equiv$ Exhaust Nozzle Pressure
$P_{\mathrm{R,\ tot}} \equiv$ Total Pressure Recovered	$\eta \equiv$ Efficiency
$P_{\infty} \equiv$ Free Stream Pressure	$M \equiv$ Mach Number

$$P_{\mathrm{R,\ tot}}(M<1) = \frac{P_{\mathrm{f}}}{P_{\infty}} \qquad \eta = \frac{P_{\mathrm{f}}}{P_{\mathrm{i}}}$$

For aircraft velocities of less than Mach 1, $P_{\mathrm{f}} \approx P_{\mathrm{i}}$; Conversely, at velocities greater than Mach 1, the cone extends to decrease the bypass ratio and optimize the lead shock position. This decelerates the intake air speed over the subsequent series of shocks, which reduces the total pressure recovery to the following relation:

$$P_{\mathrm{R,tot}}(M>1) = \eta[1 - 0.075(M-1)^{1.35}]$$

It is clear that below Mach 2, corresponding to the NASA Current Technology Goals for Future Supersonic Vehicles N+1 and N+2 objectives, this accounts for a small loss in pressure recovery. The second main propulsion performance reduction is due to spillage drag, which occurs when an inlet spills air around the lip instead of conducting it to the pressure face, as defined below:

$$D_{\mathrm{spill}} = K\big[\frac{\mathrm{d}m}{\mathrm{d}t}(V_{\mathrm{i}} - V_{\mathrm{f}}) + A(P_{\mathrm{i}} - P_{\infty})\big]$$

The relevant point is that the small engine dimensions require a small inlet frontal area, which decreases the spillage drag contribution.

Many past design features reappear on Goldeneye's engines to optimize performance. Cowl bleeds redirect incoming air through shock traps to provide subsonic cooling air to the rest of the engine, later drawn out of the nacelle by the fast-moving exhaust flowing through the ejector. For take-off and landing, where $M < 0.5$, multiple ports open along the nacelle to bring air at ambient temperature and pressure to the engine components through valves exposed to heat exchangers [50], which consist of tubular-array and micro-channel plate configurations of coolant-carrying pipes. Recent efforts, most prominently Reaction Engine's SABRE engine [51–54], have been able to reliably construct pre-cooler devices[2] composed of thousands of thin-walled, small-diameter tubes, which provide high surface area to low weight ratio made possible by advances in industrial micrometer construction. The open ports take advantage of the low pressure in the bypass channel to draw air through the tube arrays, which is chilled by small volumes of rapidly cycling coolant, decreasing the temperature of the air that is subsequently used to draw heat from the engine. This optimizes engine performance, which is beneficial for a high climbing rate out of a commercial airport with physical limitations[3].

[2]The most advanced pre-cooler devices cool intake air for hypersonic aircraft travelling at $M \geq 5$; A similar construction would be much more effective for cooling air of lower temperature during takeoff and landing.

[3]For example, San Diego International Airport has multiple restrictions due to topographical features that necessitate a steep climb rate, preventing heavier aircraft from landing.

4.4 Exhaust Nozzles

Turbojet engines offer a significant improvement over turbofans at speeds greater than Mach 1.5. They compress the entirety of the intake flow into the core, which is then energized and exhausted at high velocity and temperature to produce pure thrust. The Rolls-Royce/Snecma Olympus 593 engine took advantage of the high-speed cruise benefits of the turbojet, rendering the Concorde's propulsion as efficient as possible for the technical limitations of the time, echoed later in the Pratt & Whitney F119 and the General Electric F120 [33]. With that being said, turbofan engines excel in the high subsonic and low supersonic range, bestowing greater cruise efficiency to the design along with quieter takeoff acceleration[4]. Thus, for a flexible and commercially practical supersonic business jet, an engine that acts as both a turbofan and turbojet is optimal.

Debiasi and Papamoschou present a Targeted Mach Wave Elimination (TMWE) bypass design [31] that couples the core exhaust with a variable secondary bypass flow. This shields the mach waves produced by the turbulent eddies during the interaction of the exhaust stream with the environment, accompanied by primary bypass flow with a high bypass ratio (BPR). When the aircraft is in the subsonic and low supersonic segments of flight[5], the bypass gates (labeled A in Figure 12 below) are open, increasing the BPR to provide increased lift.

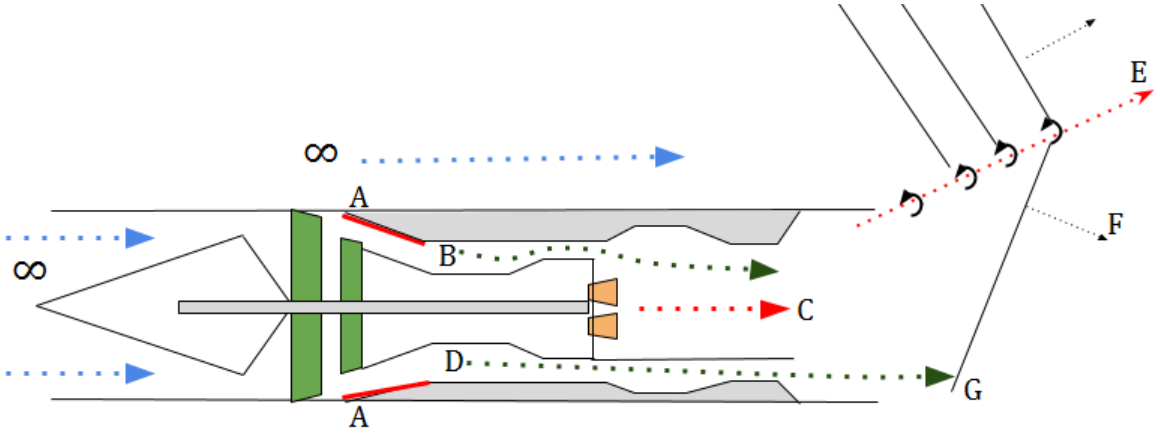

Figure 12: Diagram of the engine when the relative ambient airflow (∞) is at $M \leq 1.5$. The retracted gates, labeled A, allow flow to the bypass chambers, B is the primary bypass path, and C is the mixing of the core flow and primary bypass flow. Turbulent eddies travelling along E produce Mach waves along F. The secondary bypass flow at D suppresses the descending Mach waves at G.

[4]This is achieved by accelerating a larger mass flow at lower speed.
[5]From takeoff ($M = 0$) to transonic acceleration ($M = 1.5$).

The intake stream is then separated into core and bypass flow, the latter of which is subdivided again into a primary and secondary stream with a B:D ratio of 1.5, so that 40% of the bypass is being redirected for targeted noise suppression while 60% is harnessed to increase thrust. $\dot{m}_p$ and $\dot{m}_s$[6] are manipulated by compression and expansion completely independently, allowing the velocity difference ΔU between U_{core} and U_p to be maximized for optimal thrust. However, the ΔU between U_{core} and U_s is moderate, acting as a mediator between the core flow and the ambient flow while simultaneously suppressing the Mach waves created by the mixing of the core and primary bypass streams. This concept is put into practice with a primary nozzle placed where these two flows mix and with a secondary nozzle where the exhausts of the primary nozzle and the secondary bypass flows mix.

Debiasi and Papamoschou also show experimentally that coaxial[7] eccentric[8] nozzles are effective in mitigating downward noise originating from the elongated core of a turbojet engine [34–37]. On the following page, Figure 13 depicts the secondary flow D exhausting from the secondary nozzle and the shielding in the G region from the noise source region C. Because the secondary stream, whose velocity is closer to that of the surrounding flow, physically interferes with the mach waves, the noise is dampened and redirected such that the noise distribution with respect to arc angle has lower kurtosis[9]. The noise is therefore more evenly dissipated at lower amplitude over a large angular range, replacing the piercing scream of the turbojet with a rumble indistinguishable from other aircraft sporting turbofan engines. This is shown in Fig. 8a of [31] (not displayed). Scale model testing shows a 17% (119 to 98 dB) reduction in noise of peak noise emissions directly behind the aircraft over frequencies greater than 50 Hz, and a 3.03% (99 to 96 dB) to 9.24% (106 to 98 dB) reduction in the lateral direction from 500 to 2000Hz for an A-weighted spectrum[10].

Figure 13: A simplistic diagram of the exhaust nozzles of an engine, as viewed from behind the aircraft. The letters correspond to Figure 12; B is the primary bypass, which mixes with the core flow at C. The geometry here need not be concentric, but must be designed for optimal BRP and thrust performance at subsonic and low-supersonic ambient airspeeds. The secondary bypass flow, D, then mixes with the exhaust of the primary nozzle and is directed downwards since $\delta_v > \delta_h$, suppressing the Mach waves in the G region.

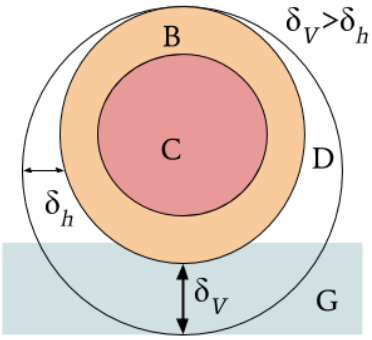

The derivation of the thrust for the TMWE design in [31] follows the Hill & Peterson approach to thermodynamic analysis [38] and non-dimensionalizes the mass flow rates in each engine component[11]. The total thrust of the engine is given by equation 25 of [31]:

$$F_{tot} = F_p + F_s = \dot{m}_p U_p + A_p(p_p - p_\infty) + \dot{m}_s U_s + A_s(p_s - p_\infty) - \dot{m}_\infty U_\infty$$

$p \equiv$ Primary Nozzle Exhaust
$s \equiv$ Secondary Airflow
$F \equiv$ Thrust
$\dot{m} \equiv$ Mass Flow
$A \equiv$ Area
$P \equiv$ Pressure
$\rho \equiv$ Density
$U \equiv$ Velocity

[6] B:$D = \dot{m}_p$:$\dot{m}_s$, where $\dot{m}_p \equiv$ primary bypass mass flow rate, and $\dot{m}_s \equiv$ secondary bypass mass flow rate.

[7] The primary nozzle is encompassed in the secondary nozzle, and often releases exhaust before the secondary nozzle.

[8] Nozzle design featuring an off-center alignment between the two coaxial nozzles along one axis. In figure 13, the primary nozzle is shifted vertically with respect to the secondary nozzle.

[9] While kurtosis is not a measurement of the flatness, sharpness, or modality of a curve (as it is sometimes misinterpreted to be), the dominant skewer of the noise distribution for a standard turbojet is not present when compared to designs featuring TMWE [31]. This means that the noise is evenly distributed at the tails of the curve, as it is in the center, and implies noise dissipation in all directions [46, 47].

[10] A noise spectrum perceived by the human ear

[11] "To compare results relative to different cycles adopting the same engine core, it is proper to non-dimensionalize the mass flow rates in each engine component with respect to the mass flow rate in the compressor." [31]

The surface areas A of the nozzles, considered over a vertical plane, are defined by eqns. 23 and 24 of [31]:

$$A_p = \frac{\dot{m}_p}{\rho_p U_p} = \frac{\dot{m}_{com} m_{r_p}}{\rho_p U_p}$$
$$A_s = \frac{\dot{m}_s}{\rho_s U_s} = \frac{\dot{m}_{com} m_{r_s}}{\rho_s U_s}$$

where *com* represents the compressor. Pressure is calculated by $P = \rho RT$, where $\rho = \frac{m}{v}$ is the density, R is the gas constant, and T is the temperature at the location of interest. The nozzle exit velocity is defined by equation 22 of [31], $U = M\sqrt{\gamma RT}$, where M is the Mach number and $\gamma = \frac{c_p}{c_v}$ is the specific heat ratio. The corrected compressible mass flow rate is then given by equation 1 of [39]:

$$\dot{m} = \frac{AP_{\text{tot}}}{\sqrt{T_{tot}}}\sqrt{\frac{\gamma}{R}}M\left(1 + \frac{\gamma - 1}{2}M^2\right)^{-\frac{\gamma+1}{2(\gamma-1)}}$$

Alternatively, the corrected compressible mass flow rate, equation 2 of [39], can be used by dividing by a factor of $g = 9.81$ m/s^2 and by considering the temperature ratio, $\Theta = \frac{T}{T_\infty}$, and the pressure ratio, $\delta = \frac{P}{P_\infty}$, yielding: $\dot{m} = \frac{\dot{W}\sqrt{\Theta_t}}{gA\delta_t}$, which for air computes to:

$$\dot{m} = \frac{1}{g}0.59352M(1 + 0.2M^2)^{-1}\zeta_{\dot{m}}\frac{\text{kg}}{\text{s } m^2}$$

where $\zeta_{\dot{m}} = 70.3069\frac{\text{lb}}{\text{s in}^2}\frac{\text{s m}^2}{\text{kg}}$ is the unit conversion factor for mass flow from American to SI units.
The assumptions made to calculate the total thrust capability of each engine are as follows. The gas constant of air does not significantly differ in the temperature range of 300-1500 K nor in the pressure range of air in the altitude range of 0-20 km [40–42].

Name	Abbreviation	Valves Open	Valves Closed	Source
Acceleration due to gravity	g	9.81 $\frac{\text{m}}{\text{s}^2}$	-	[d]
Mach number of primary flow velocity (M)	M_p	5	4	[31]
Temperature of primary flow (K)	T_p	1800	1700	[43–45]
Mach number of secondary flow velocity (M)	M_s	0.4	-	[31]
Temperature of secondary flow (K)	T_s	550	N/A	[a]
Ratio of primary to secondary bypass volumes.	U_p:U_s	10:1	$U_p : 0$	[a]
Ambient air velocity (M)	U_∞	0.4	1.8	[a]
Average specific heat ratio	γ	1.36	-	[31]
Gas constant of air ($\frac{\text{J}}{\text{kg} \cdot \text{K}}$)	R	287	-	[40–42].
Density of air at 0 km elevation ($\frac{\text{kg}}{\text{m}^3}$)	ρ_∞	1.225	-	[40]
Density of air at 20 km elevation ($\frac{\text{kg}}{\text{m}^3}$)	ρ_∞	0.089	-	[40]
Temperature of air at 0 km elevation (K)	T_∞	300.00	-	[a]
Temperature of air at 20 km elevation (K)	T_∞	216.65	-	[41]

[a]≡assumed, [d]≡datum.

Table 1: Parameters used for the thrust, exhaust nozzle area, and mass flow calculations.

Figure 14 conveys the relationship between the cross sectional areas of the primary and secondary exhaust nozzles. When the bypass valves are open to the secondary bypass (at subsonic, transonic, and low supersonic

speeds) the maximum thrust value is increased by a greater secondary bypass, shown in 15a. However, the thrust relation in 15b requires a large primary nozzle area. Optimizing the surface area of the primary and secondary exhaust nozzles results in a ratio of $\frac{A_p}{A_s} \approx 1.4 = 3.5/2.5$. As discussed in Section 4.1, the total diameter of each engine must be 0.684 m, implying that the combined nozzle area must be 1.469 m^2 for a circular cross section. Therefore, the cross sectional areas are 0.857 m^2 for primary exhaust nozzle and 0.612 m^2 for the secondary nozzle. The secondary nozzle does not require exorbitant modifications to current exit nozzle designs, and its modest area requirement allows it to fit tidily underneath the primary nozzle, eliminating any significant deviations from well tested exit nozzle designs.

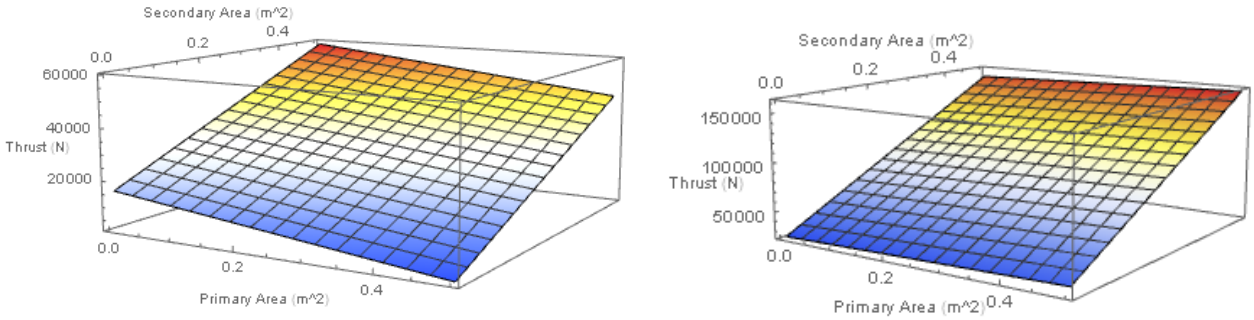

(a) Secondary bypass open.

(b) Secondary bypass closed.

Figure 14: Thrust in Newtons as a function of primary exhaust nozzle area and secondary bypass area. Note that since $\dot{m} \propto \frac{1}{\text{BPR}}$, the optimization lies in the ratios that will give a maximum thrust when the bypass valves are (a) opened for increased lift at $M \leq 1.5$, and (b) closed for supersonic cruise (BPR = 0).

For the TMWE, velocity is inversely related to the thrust whether or not the secondary nozzle is active, as visible in Figure 15. The values are independently calculated for the two engines, so thrust is assumed to combine linearly. In both velocity ranges, the maximum thrust of each engine exceeds the previously calculated cruise thrust of 10.861 kN by a large margin. At takeoff, a 28.053 kN thrust yields a 17.192 kN margin of increased lift, allowing for a shorter runway and opening up the ability for Goldeneye to access airports used by small business jets. Less thrust during takeoff and landing, reduces noise emissions, easing permission-of-use discussions with authoritative bodies from communities near airports (city and state governments, noise pollution committees, etc.).

Increased thrust is required in the transonic region, which must be traversed quickly to avoid high fuel costs associated with the spike in drag. A thrust of 27.227 kN at $M_\infty = 0.8$ and a thrust of 26.840 kN at $M_\infty = 1.0$ give a margin of roughly 16 kN per engine in the transonic range. At cruise velocities of Mach 1.6-1.8, the thrust ranges from 25.191 kN to 25.589 kN, giving 14.728 kN to 14.330 kN of additional available thrust. While this is less than when the secondary bypass is active, there is also less need for additional thrust, excluding emergencies. At all velocities, it is possible to sustain the cruise thrust with some additional thrust remaining. In the case of an engine failure while at supersonic speeds, the second engine sustains stable supersonic flight until the aircraft is safely brought out of the supersonic range. The increased thrust at subsonic speeds allows for a longer range, allowing the aircraft to safely reach airports in the event of an engine failure over the ocean.

4.5 Materials

The engine intake fan must withstand all weather conditions and foreign object ingestion. As the engines are mounted on top of the fuselage, there is reduced risk from debris on taxiways and runways, but the possibility of bird strike is still a concern. During operation, fan blades are subject to intense tensile stress and therefore must be strong and corrosion-resistant, as well as light to minimize the fan's moment of inertia. However, relative to other engine components, the intake fan does not experience extremely high temperatures, and does not carry as strict of a temperature requirement. Precipitation-hardened 6061 aluminum provides the necessary creep and corrosion resistance, while having an excellent strength-to-weight ratio.

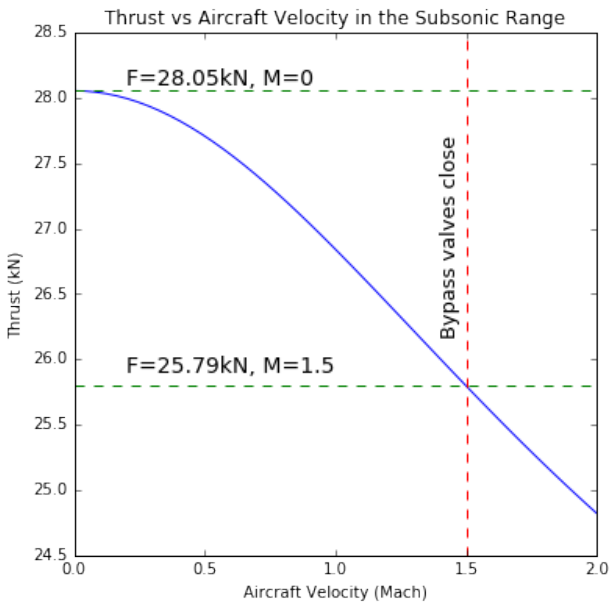

(a) Secondary bypass open.

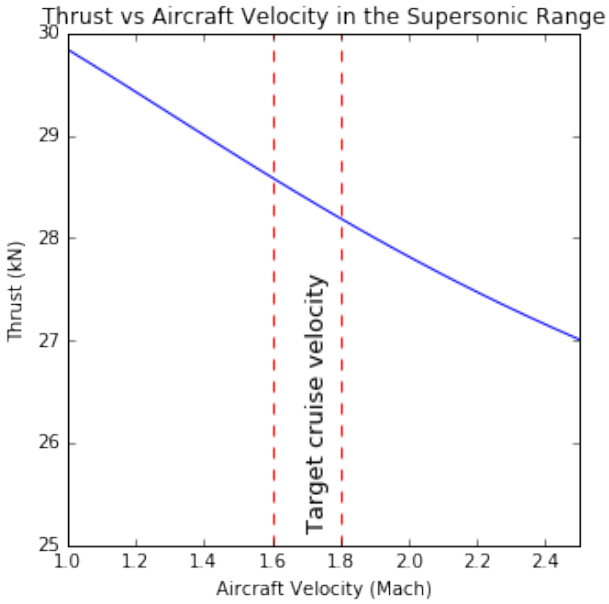

(b) Secondary bypass closed.

Figure 15: Thrust in Newtons as a function of velocity of the aircraft for a single engine. At all velocities the thrust exceeds the cruise requirements, and is capable of a thrust increase of 255% for take-off and landing; To calculate the total thrust, both the engines must be accounted for.

On the other hand, the turbine fan imposes a vastly different set of design challenges. Temperatures inside the turbine may reach excess of 1000 °C, and the tremendous angular velocity of the fan imposes extreme tensile loads on the blades. In this environment, deformation from creep, a temperature-dependent process, becomes a major issue. Traditionally, turbines have been fabricated from nickel-based superalloys such as Nimonic and Inconel. Inconel 792 is precipitation-strengthened and very resistant to creep and corrosion at high temperatures, making it an attractive option for the turbine fan blades.

Another approach to combating creep is to enlarge the grain boundaries in the material, minimizing the net diffusion of atoms along them, which is responsible for localized slipping. Turbine blades can be manufactured from a single crystal, so that they effectively contain no grain boundaries. This removes the mechanism of action for Coble creep and eliminates the risk of weakened grain boundaries by corrosion. Single crystals of superalloys such as CMSX-6 have been harvested to make turbine fan blades, making them another smart choice for this component [30].

The combustion chamber operates under similar conditions to the turbine, at even greater temperatures. Because there is no stress from rapidly moving parts, high-temperature alloys that are corrosion-resistant even at high temperatures, such as Ti-5553, are suitable. Ti-5553 is easily castable, making the manufacturing of the complex geometries in combustion chambers possible. Furthermore, temperatures within the combustion chamber can be controlled by careful planning of air cooling techniques. In addition, coatings derived from zirconium dioxide or yttrium oxide provide thermal insulation at the surface without sacrificing the ductility of the alloy.

5 Design Implementation

5.1 Wing Size

A wing geometry was parametrized in section 2.3, outlining a planform wing shape based on the root chord-length (R), the leading edge's sweep angle (Λ), and the trailing edge's sweep angle (Λ_{rear}). To produce a final wing shape and size, these parameters were varied to create optimal conditions in supercruise flight, and during take-off and subsonic flight. As was outlined in the previous section, the optimal leading and trailing sweep angles were set as $\Lambda = 60°$ $\Lambda_{rear} = 60°$. A decrease of the leading angle would result in a higher aspect ratio and provide more lift, at the expense of the leading edge crossing paths with oblique shock waves. An increase of the trailing angle would also result in a larger clipped-delta geometry for supersonic flight, but would decrease the size of the radial extender, thus impacting subsonic flight performance. After performing around 25 flow simulations at both supercruise and standard temperature-and-pressure conditions in the Solidworks 2017 Flow Simulation Package, it was found that compromises to either of these angles were not necessary to enable highly-efficient supersonic flight. The remaining parameter, the Root chord length was varied to scale the wing. This finalized the size of the wing to match a fully loaded Goldeneye AB1 in lift.

The behaviour of laminar airfoils is analogous to that of the centerboard or keel of a sailboat, the flow around it is streamlined and relatively symmetrical when compared to a conventional airfoil. As such it will not provide much lift when its angle of attack, or incidence angle, is set to zero. However, when agitated some force, causing an infinitesimal rotation, it will respond strongly to counter this force. To study this behaviour, prototypes with root chords varying from 8 to 20 meter in length were subjected to a flow moving at Mach 1.7 with small incidence angles ranging from 0 to 3 degrees in the Flow Simulator. To validate the model, a replica CAD was created of the Concorde's wing, and the results of flow studies on it were compared to Concorde flight data. It was found that the model's numerical findings did not correlate strongly with validated data, but they did follow the general trends that were expected. This is attributed to the fact that the Solidworks Flow Simulator is not optimized for supersonic flow or airfoil analysis.

As this paper outlines the conceptual design of the Goldeneye AB1, some approximations need to be made to find the fully loaded aircraft mass. The Gulfstream G280 was chosen as a reference aircraft for this approximation. It's maximum capability weight is 17962.2 Kg, or 176030 N. As it is designed to handle 20 passengers, 8 more than the AB1, over similar ranges, an absolute upper bound of the AB1's capacity load is chosen to be 75% of the Gulfstream's weight. This takes into account the smaller size of the AB1, its lighter materials, and a larger fuel capacity. The lift was found to increase exponentially, and approximately linearly for small incidence angles. Although the simulation of the Concorde wing predicted a lift to drag ratio that was about 40% of the actual ratio, it was found that the maximum weight was matched by various prototype wing sizes at flow incidence angles between 0.5° and 1.7°. Considering the lower predicted performance of the Concorde model, these results are considered excellent validations of the wing design, as the actual pitch angle of the aircraft to maintain this lift will likely be much lower than the found values. The root chord length was established at R = 15m to optimize the lift characteristics. This chord length gives the AB1 a similar planform area to the Aerion Supersonic jet, however the Aerion lacks the high lift characteristic of the Ab1's variable geometry at low speeds. The minimum drag on this wing (including both the starboard and portside wing) at Mach 1.7 was found to be around 3000N. At STP, a pitch angle of 10°, and a takeoff velocity of 300 km/h, deployment of the radial extender increased the total lift generated by the wing by about 45%. This is attributed to the increase in planform area, and to the larger resistance to flow separation at large incidence angles of the extended Ogival Delta. It is more resistant to this separation since a larger chord results in lower absolute curvature on the wing. Considering the reduction in lift predicted by the simulator, this is considered a highly promising concept.

5.2 Canard and Vertical Stabilizer

The AB1's canard is modeled after the Eurofighter Typhoon's, a foreplane approximately one third of the wing area featuring a full-span slotted elevator for pitch control. The canard is placed on the nose just in front of the cockpit to form a closely coupled configuration, lying forward and slightly above the wings. A canard mounted above the wings provides a greater pitching moment for a given angle of attack (Figure 16b), which

is desirable since the foreplane is the prime control surface for the aircraft's pitching moment. Furthermore, the close-coupled configuration provides greater lift during takeoff and landing as well as during supercruise [28]. The top mount of the canard inhibits it from destabilizing the flow over the wing at supersonic speeds as well. At low speeds, the canard's surface directs airflow downwards over the wing, and at high angles of attack induces a wake vortex that attaches to the upper surface of the wing. This in turn generates vortex lift, delaying stall and stabilizing airflow over the wing. [29].

The canard planform is a truncated, 45° clipped delta shape, selected for its high lift coefficient and lift-to-drag ratio (See Figure 16a). The AB1's canard features the same NACA 66-206 airfoil as the wings because this profile satisfies the desired laminar flow separation in the supersonic region.

A vertical stabilizer was added in between the engine mounts to provide yaw stability and control. The airfoil selected for the stabilizer is the NACA 64-008A Airfoil, a symmetrical and highly laminar airfoil with a thickness ratio of 8%. The airfoil was selected for its low drag and laminar flow. The current implementation includes a generic arrow shaped wing, however this could be optimized to a more efficient supersonic design in future.

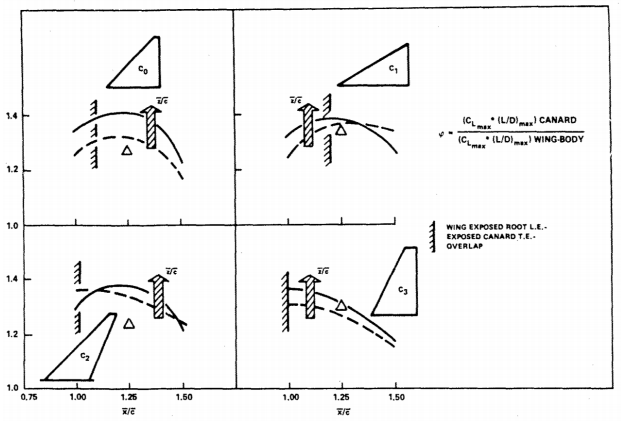

(a) Product of lift-to-drag ratio and maximum lift coefficient for various canard shapes [55].

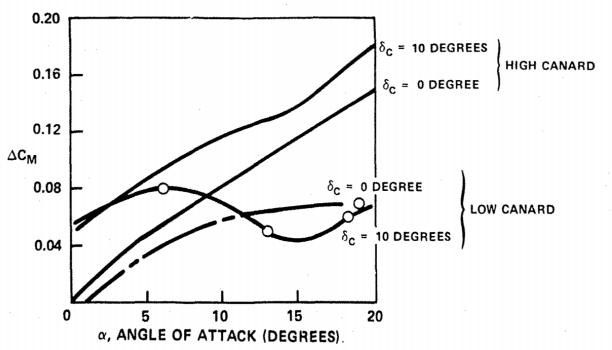

(b) Pitching moment coefficient with respect to angle of attack for high and low canards [55].

Figure 16: Thrust in Newtons as a function of velocity of the aircraft for a single engine. At all velocities the thrust exceeds the cruise requirements, and is capable of a thrust increase of 255% for take-off and landing; To calculate the total thrust, both the engines must be accounted for.

5.3 Engine Mount

Goldeneye's engines are be mounted on top of the fuselage toward the rear of the aircraft. As previously discussed, this reduces the noise produced by the engines, using the wings as a sound barrier without subjecting them to high thermal stresses. The engines are encased by a nacelle that is blended into the top surface of the wing and is partitioned into two sections to optimize air intake for both engines.

6 Performance Criteria

6.1 Fuel Efficiency and Range

To find a baseline for the specific fuel consumption (SFC) of the engines, the Concorde's efficiency at supersonic cruise can be scaled accordingly. Particularly, the efficiency of the Olympus engines varies linearly with velocity [22]. At Mach 2.2, the Olympus engines have a $SFC = 1.195$. Therefore, at a speed of Mach 1.7, Goldeneye has a $SFC = 0.923$ a baseline efficiency that does not account for the additional performance improvements due to the variable geometry intake. Given this value, a lower bound for Goldeneye's range can be estimated using the Bregeut Range Equation [25]:

$$\text{Range} = \frac{v \cdot \frac{C_L}{C_D}}{g \cdot SFC} \cdot \ln\left(\frac{W_{\text{initial}}}{W_{\text{final}}}\right)$$

where v is velocity, g is the acceleration due to gravity, W_{initial} is the initial weight of the aircraft, and W_{final} is its final weight. Estimating that $\frac{W_{\text{initial}}}{W_{\text{final}}}$ is 1.5, meaning the plane carries half as much of its dry weight in fuel, is reasonable because this value is true of many business jets currently in service, including the Gulfstream G280 [24].

Therefore, the Goldeneye's range is calculated to be 4227 km.

6.2 High Lift for Takeoff and Landing

The two features responsible for high lift are the high delta-shape canard and the ogival delta wing, the latter providing additional lifting surface area at low speeds to take advantage of wake vortices generated by the leading edge of the wing. This is necessary given that the clipped delta wing configuration fails to deliver sufficient lift during takeoff and landing speeds. Moreover, at high angles of attack additional wake turbulence is generated by the canard, which increases the speed of airflow on the top surface of the wing. The canard is also responsible for creating a downwash at its trailing edge that directs airflow over the top surface of the wing, consequently generating lift at supersonic speeds.

7 Feasibility

Up to now, private ventures have spearheaded the attempt to reintroduce commercial supersonic flight. In the business sector, Boom, Aerion, and Spike are noteworthy companies that are producing supersonic business jets, though these are currently concept aircraft awaiting completion. Engine giant Rolls-Royce recently revealed plans to develop new supersonic engines, prompting aircraft makers to roll out candidate aircraft [56]. Market trends yield tentative promise for the growth of supersonic business jets. A market analysis run by the German Aerospace Center revealed "200 of the largest, heaviest and most expensive jets are sold per year, and this segment is thought to have the greatest growth potential. Diverse market analysis justify starting a SSBJ (supersonic business jet) development with a yearly demand of about 20 SSBJs. [57]" Moreover, just last year Aviation Week reported that the SSBJ market is anticipated to reach $3 billion by 2020, with an annual growth of 4% [58]. These figures coupled with predicted market growth are promising for AB1's future in the industry.

The feasibility of developing Goldeneye comes down to the design challenges, developmental roadblocks, and money. The economics of the AB1 can be broken down into research and development costs, customer pricing, material costs, and construction costs.

7.1 Propulsion Systems

Goldeneye is propelled using an offshoot of a tried and true engine. Thus, many of the biggest engineering challenges that face its development have already been solved problems by decades of R & D leading up to the Concorde's release. The development and installation of the modified Olympus 610 engine could be done in conjunction with Rolls-Royce, with whom collaboration would significantly financially aid Goldeneye's team.

The Concorde eventually became commercially impractical because of its high fuel consumption, which severely limited its profitable operation by parent airlines. Goldeneye overcomes this challenge in several different ways. Its Mach 1.7 cruise speed is lower than that of the Concorde, which lowers specific fuel consumption right off the bat. Other advancements are also applied to the propulsion systems of Goldeneye, include a spike intake, improved bypass design, and afterburner usage only while breaking the sound barrier, as discussed in Section 4.

A key observation about these improvements is that Goldeneye need only incorporate existing technology into its propulsion system. This results in a direct reduction of research and development costs. More importantly,

these improvements improve fuel efficiency, reducing prices and further contributing to Goldeneye's commercial viability.

7.2 Wing Systems

The most significant implementation challenge of the AB1 is its retracting wing panel. The wing's internal structure is heavily loaded by the panel and tracks, which may be subject to jams and actuation failure. To address this issue, regular servicing of the mechanism is essential to minimize the risk of mechanical failure. From a material cost standpoint, the use of components such as titanium spars and fasteners, as previously discussed earlier, may drive up fabrication costs compared to those of Goldeneye's subsonic counterparts. With that being said, recent manufacturing advancements may facilitate ease of production for the required components. Selective Laser Sintering (SLS) can be used to rapidly prototype and test the system. This process consists of fusing loose metal particles together by scanning a laser over points in space to form a desired three-dimensional part, enable swift integration of parts while reducing production costs [60].

With cost considerations in mind, Goldeneye AB1 seeks to take advantage of common aerospace alloys and other materials. As such, manufacturing facilities would not require extensive retooling or other modifications. The fuselage's Ti-6Al-4V alloy is used extensively outside of the aerospace industry for biomechanical and chemical applications. Its ubiquity and supply serves to reduce costs across the board, from bulk material purchasing to manufacturing. Similarly, 7075 aluminum, found in the wing spars and ribs, and 6061 aluminum, found in the engine intake fan and other internal elements, have long, distinguished histories in aircraft construction. Their relatively low cost and high reliability make them well suited for production. Inconel 792, used in the turbine fan, is a sand-castable alloy, produced by a method that allows for the fabrication of complex geometries in a much more affordable manner than comparable processes. Ti-5553, in the engine combustion chamber, is also easily castable. By purchasing common, high-quality materials in bulk, production and maintenance costs of the AB1 can be significantly reduced.

7.3 Comparison With Existing Business Jets

A good indicator of the feasibility of a product is a comparison to similar products in the industry. The table below provides a useful baseline to judge the AB1 by several important factors against some common planes.

Plane	Mach Speed	Range(nm)	Fuel Efficiency (SFC)	Passengers
Goldeneye	1.7	4227	0.923	12
Cessna Citation Sovereign+	0.68	3063	0.391	9-12
Gulfstream G280	0.84	3600	0.642	10-19
Cessna Citation X	0.91	3370	0.39	12
Challenger 350	0.83	3200	0.406	9
Embraer Legacy 500	0.83	3125	0.406	8-12
Challenger 650 CL-604	0.68	3714	0.69	10-19

Two key observations can be made from the above table. First, Goldeneye's speed is more than twice that of most comparable business jets, and has a greater range. A flight from London to New York would take $3.5 - 4$ hours, half the time it currently takes to complete the trip on a passenger jet. The main appeal of the Concorde was its reduction of travel times, and because Goldeneye is tailored for business travel, it remains an enticing option for those with enough money to afford it.

8 Conclusion

8.1 Design Goals

All required technical design features are matched by the Goldeneye SSBJ, the most obvious being the cruise speed of M=1.6-1.8 and payload of 12 passengers, as the design was build from the ground up to match these parameters. With a TSFC of 0.93 and the engines supplying 4883.29 lbf (21722N) of thrust to cover the

maximum range of 4227nmi in 3.961 hours at Mach 1.6 (1066.78 knots), a flight requires 17,853 lbs of fuel, or 2.84 passenger-miles per pound of fuel, far exceeding the requirement of 1.00 passenger-miles per pound of fuel at cruise conditions; These conditions consume 35.204% of the amount of fuel that could be consumed while still achieving the fuel efficiency goal.

The take-off field length is, for the sake of calculation, divided into two segments, takeoff ground roll and horizontal range required to climb to 35ft. The former is defined as follows.

$$d_{TO} = \frac{m_{TO} \cdot (v_{LO} - v_W)^2}{2 \cdot (F_{TO} - D_{TO} - \mu \cdot (m_{TO} \cdot g - L_{TO}) - m_{TO} \cdot g \cdot \sin\gamma)}$$

$d \equiv$ Distance
$v \equiv$ Velocity = 155kts
$m \equiv$ Mass = 17962kg
$F \equiv$ Thrust = 40000N (Cruise + 18278N)
$D \equiv$ Drag = 29410kN
$\mu \equiv$ Coefficient of friction = 0.71
$L \equiv$ Lift = 480kN
$\gamma \equiv$ Runway slope = 0°
Subscript $TO \equiv$ Takeoff
v_W = Wind Speed

For a preliminary calculation, the runway is taken to be perfectly flat and the wind to be 0 knots, which when calculated yields a takeoff ground roll of 1138.07m, or 3373.83ft. To use the remaining 3626.17ft of runway left to clear the 35ft FAA takeoff screen, Goldeneye must climb at an minimum angle of 0.55°. A comfortable climb angle of 10° clears the end of the runway by a vertical distance of 639.392 ft, and a maximum climb angle of 15° gives 971.63 ft of vertical clearance.
Goldeneye's highly fuel-efficient and noise mediated design relies on novel concepts with exclusively realistic forecasts, leaving ample time for finalized component development, prototyping, and market maturation. However, an IOC of 2025 designates the 7 years from 2018 to 2025 to developing the concept into a passenger-ready, fully-marketable business aircraft, a small figure when compared to the current paradigm of commercial aircraft design. For example, the Boeing 787, a technical feat but still completely abiding by the tried-and-tested modern commercial subsonic, turbofan engine, lower wing mount, passenger airplane scheme, took 8 years and 9 months to develop[12] It should be recognized that there exists a possibility of the IOC being a later date if the research and development stage is not complete by 2020, the prototype by 2022, and the first complete, full-scale aircraft by 2024; The primary expected reason for this is inadequate funding.

8.2 Future of Industry

Since the latter portion of the twentieth century and decline of the space race era, innovation in aerospace has remained stagnant. The Concorde, introduced in 1969 and retired from service in 2003, is the closest feat humans have attained in commercially travelling supersonic. Since then, we have regressed. The aerospace industry today through private conglomerates such as SpaceX, Boeing, and Lockheed Martin, is pivoting towards space exploration and interplanetary travel, and focusing less on furthering aviation on Earth. Moreover, with faster and sustainable forms of transportation being developed (Elon Musk's Hyperloop, Vahana by A^3, etc.), the appeal of subsonic flight is diminishing. To remain relevant, aviation must undoubtedly evolve into the supersonic regime. Goldeneye AB1 is envisioned as a galvanizing platform for supersonic travel. Coupled with present-day technological advances, the unconventional design implementations aboard the business jet seek to vanquish historical challenges of supersonic travel, and ultimately pave the road to supersonic flight for all.

[12] The 7E7 program was officially announced on January 9, 2003, received its type certificate on August 26, 2011 and flew the first passenger flight for revenue on October 26, 2011. This of course includes the economic recession from December 2007 to June 2009.

References

[1] Kumar, M., Kannan, M., Kumar, V., Manigandan, A., Praveen, G. "Analysis of Shock over NACA 66-206 at Supersonic Regime". Advances in Aerospace Science and Applications, Vol. 3, No. 2, pp. 125-130, Hindustan University, Padur, India, 2013.
https://www.ripublication.com/aasa/aasav3n2spl_16.pdf

[2] Wang, F., Milanovic, I., Zaman, K., Povinelli, L. "A Quantitative Comparison of Delta Wing Vortices in the Near-Wake For Incompressible and Supersonic Free Streams". J. Fluids Eng 127(6), 1071-1084, July 12, 2005.
http://fluidsengineering.asmedigitalcollection.asme.org/article.aspx?articleid=1430232

[3] Kroo,I: "Unconventional Configurations for Efficient Supersonic Flight." Stanford University June 6, 2005. Page 13.
http://aero.stanford.edu/reports/vki_kroo_supersonics.pdf

[4] Sadraey, Mohammad: "Aircraft Design: A Systems Engineering Approach." Chapter 5. Wiley, 2012. Page 176.
http://www.academia.edu/4573651/Wing_Design_i_Chapter_5_Wing_Design_Mohammad_Sadraey

[5] Sadraey, Mohammad: "Aircraft Design: A Systems Engineering Approach." Chapter 5. Wiley, 2012. Page 235,239.
http://www.academia.edu/4573651/Wing_Design_i_Chapter_5_Wing_Design_Mohammad_Sadraey

[6] Sadraey, Mohammad: "Aircraft Design: A Systems Engineering Approach." Chapter 5. Wiley, 2012. Page 205
http://www.academia.edu/4573651/Wing_Design_i_Chapter_5_Wing_Design_Mohammad_Sadraey

[7] Sadraey, Mohammad: "Aircraft Design: A Systems Engineering Approach." Chapter 5. Wiley, 2012. Page 224
http://www.academia.edu/4573651/Wing_Design_i_Chapter_5_Wing_Design_Mohammad_Sadraey

[8] Mason, W.H.: "Supersonic Aerodynamics." Virginia Tech. 7/31/2016. Chapter 10, page 20.
http://www.dept.aoe.vt.edu/ mason/Mason_f/ConfigAeroSupersonicNotes.pdf

[9] Mohan Kumar G, Manoj Kannan G, Vignesh Kumar R, Manigandan A, and Praveen G: "Analysis of Shock over NACA 66-206 at Supersonic Regime." Advances in Aerospace Science and Applications. ISSN 2277-3223 Volume 3, Number 2 (2013), pp. 125-130
https://www.ripublication.com/aasa/aasav3n2spl_16.pdf

[10] Jones, Robert T: "Report 1284: Theory of Wing-Body drag at Supersonic Speeds." NACA Cranfield, United Kingdom. 1956.
http://naca.central.cranfield.ac.uk/reports/1956/naca-report-1284.pdf

[11] Sadraey, Mohammad: "Aircraft Design: A Systems Engineering Approach." Chapter 5. Wiley, 2012. Page 223.
http://www.academia.edu/4573651/Wing_Design_i_Chapter_5_Wing_Design_Mohammad_Sadraey

[12] ConcordeSST.com: "Concorde Technical Specs: Fuel system."
http://www.concordesst.com/fuelsys.html

[13] Hall, Nancy: "Center of Pressure." NASA, Glenn Research Center.
https://www.grc.nasa.gov/WWW/k-12/airplane/cp.html

[14] Cornei, Simona: "Mach number, relative thickness, sweep and lift coefficient of the wing - An empirical investigation of parameters and equations." Department of Automotive and Aeronautical Engineering, Hamburg University of Applied Sciences. 31/05/2005.
http://www.fzt.haw-hamburg.de/pers/Scholz/arbeiten/TextCiornei.pdf

[15] NACA 66-206
http://airfoiltools.com/airfoil/details?airfoil=naca66206-il

[16] Araujo, G., Almeida, S."Design Procedure for a Fowler Flap Mechanism". 18th International Congress of Mechanical Engineering, Ouro Preto, Brazil, November 2005.
http://www.abcm.org.br/anais/cobem/2005/PDF/COBEM2005-0040.pdf

[17] Grumman F-14 Tomcat
https://en.wikipedia.org/wiki/Grumman_F-14_Tomcat#Variable-geometry_wings_and_aerodynamic_design

[18] Concorde Elevons and Rudders
http://www.heritageconcorde.com/concorde-elevons-and-rudder

[19] Interference Drag of Wing Mounts
Sadraey, M. H., Wing Design, in "Aircraft Design: A Systems Engineering Approach", John Wiley & Sons, Ltd., Chichester, UK, 2012, pp. 12

[20] Sears-Haack Body
Ashley, H., Landahl, M., "Aerodynamics of Wings and Bodies", Addison-Wesley, 1965.

[21] Airplane Aerodynamics and Performance, Roskam Jan and Lan C E

[22] Propulsion and Efficiency, SMU Lyle School of Engineering
http://lyle.smu.edu/propulsion/Pages/efficiency.htm

[23] Aircraft Performance, MIT OCW
ocw.mit.edu/ans7870/16/16.unified/propulsionS04/UnifiedPropulsion4/UnifiedPropulsion4.htm

[24] Gulfstream G280 Specifications
gulfstream.com/aircraft/gulfstream-g280

[25] Bregeut Range Notes, Fall 2008, MIT
web.mit.edu/16.unified/www/FALL/Unified_Concepts/Breguet-Range-U2-notes-Fall08(2).pdf

[26] Saturn V Launch Simulations
braeunig.us/apollo/saturnV.htm

[27] Aspects of Aircraft Design and Control, Olivier Cleynen, May 2014
documents.ariadacapo.net/cours/aspects_aircraft_design/lecture_8.pdf

[28] Anderson, Seth B. "A Look at Handling Qualities of Canard Configurations". NASA, September 1986.
https://ntrs.nasa.gov/archive/nasa/casi.ntrs.nasa.gov/19870013196.pdf

[29] "Jet Aircraft – Effect of a close-coupled canard on a swept wing". SAI Research Report (Abstract). Sage Action, 2009.
http://www.sageaction.com/aircraft_testing1.htm#JetAircraft

[30] Onyszko, A., and Kubiak K., "Method for Production of Single Crystal Superalloys Turbine Blades", *Archives of Metallurgy and Materials*, Vol. 54, No. 3, 2009, pp. 765-771.

[31] Debiasi, M., and Papamonschou, D. "Cycle Analysis for Queiter Supersonic Turbofan Engines", University of California, Irvine, 2001.

[32] Papamoschou, D., and Debiasi, M., "Directional Suppression of Noise from a High-Speed Jet", *AIAA Journal*, Vol. 39, No. 3, 2001, pp. 380-387.

[33] Sweetman, B., "YF-22 and YF-23 Advanced Tactical Fighters", Motorbooks International, 1991, Osceola, WI, pp. 61-64.

[34] Murakami, E., and Papamoschou, D., "Mixing Layer Characteristics of Coaxial Supersonic Jets", *AIAA Journal*, 2000-2060.

[35] Papamoschou, D., "Mach Wave Elimination from Supersonic Jets" *AIAA Journal*, Vol.35, No.10, 1997, pp.1604-1611

[36] Papamoschou, D., and Debiasi, M., "Noise Measurements in Supersonic Jets Treated with the Mach Wave Elimination Method",*AIAA Journal*, Vol. 37, No. 2, 1999, pp. 154-160.

[37] Debiasi, M., and Papamoschou, D., "Noise from Imperfectly Expanded Supersonic Coaxial Jets", *AIAA Journal*, Vol.39, No.3, 2001, pp.388-395.

[38] Hill, P., and Peterson, C., "Mechanics and Thermo dynamics of Propulsion", 2nd Ed., Addison Wesley, 1992, New York

[39] Space Flight Systems, Glenn Research Center, Online Educational Material: Corrected Airflow per Area

[40] Cengel, Yunus A., and Boles, Michael A. Thermodynamics: An Engineering Approach. New York, NY: McGraw-Hill, 2011. Print.

[41] Sontag, Borgnakke and Van Wylen. Fundamentals of Thermodynamics. 6th Ed., John Wiley & Sons, Inc., 2003. Print.

[42] Kittel, C., and Kroemer, H. Thermal Physics. 2nd Ed., W.H. Freeman, 1980. Print.

[43] Jackson, P.A. "Jane's all the World Aircraft, 1998-1999", Sentinel House, 1998, Couldson UK.

[44] Roth, B., and Mavris, D., "Analysis of Advanced Technology Impact on HSCT Engine Cycle", AIAA Pap er No. 99-2379, 1999.

[45] Sanghi, V., and Lakshmanan, B.K., "Some Trends in Engine Cycle Selection and Overall Aircraft Sizing", Proceedings of the XIV International Symposium on Air Breathing Engines, ISABE pap er 99-7112, 1999.

[46] Freedman, D., Pisani, R., and Purves, R. "Statistics". 4th Ed., W.W. Norton & Company, 2007.

[47] Devore, J. L. "Probability and Statistics for Engineering and the Sciences". 8th Ed., Cengage Learning, 2011.

[48] American Environment Company, Inc. "Acoustic Power and Sound Pressure Levels of Typical Noise Sources". Medford, N.Y., 2017.

[49] "Inlet Performance", NASA Glenn Research Center, edited by Nancy Hall, 2015.

[50] Webber, H., Feast, S. and Bond, A. "Heat Exchanger Design in Combined Cycle Engines" IAC-08-C4.5.1, 2008.

[51] Mehta, U., Aftosmis, M., Bowles, J., & Pandya, S. "Skylon Aerodynamics and SABRE Plumes". 20th AIAA International Space Planes and Hypersonic Systems and Technologies Conference., Glasgow, Scotland, 2015

[52] Musielak, D. "SABRE: A high speed air breathing rocket engine fo the SSTO SKYLON spaceplane". 2012.

[53] Varvill, R. and Bond, A. "The Skylon Spaceplane: Progress to Realization". JBIS, Vol. 61, pp. 412-418, 2008.

[54] Aggarwal, R., Lakhara, K., Sharma, P.B., Darang, T., Jain, N., Gangly, S. "SABRE Engine: Single Stage to Orbit Rocket Engine".

[55] Lacey, D,. "Aerodynamic Characteristics of the Close-Coupled Canard as Applied to Low-to-Moderate Swept Wings". Vol.1, David W. Taylor Naval Ship Research and Development Center, Bethesda, MD, 1979.
`http://www.dtic.mil/dtic/tr/fulltext/u2/a063819.pdf`

[56] Rolls-Royce Is Ready For A Supersonic Business Jet
https://airinsight.com/2017/04/10/rolls-royce-ready-supersonic-business-jet/

[57] Liebhardt, B., Lütjens, K. "An Analysis Of The Market Environment For Supersonic Business Jets". German Aerospace Center-Air Transportation Systems. Hamburg, Germany, 2011.
http://elib.dlr.de/75275/1/DLRK2011_Liebhardt-L%C3%BCtjens.pdf

[58] Supersonic Business Jet Market Expected To Grow 4% Annually
http://aviationweek.com/awin-only/supersonic-business-jet-market-expected-grow-4-annually

[59] Shama Rao, N., Simha, T. G. A., Rao, K. P., Ravi Kumar, G. V. V. "Carbon Composites Are Becoming Competitive and Cost Effective". Infosys.

[60] Selective Laser Sintering
https://en.wikipedia.org/wiki/Selective_laser_sintering#Advantages_vs._disadvantages